

Towards dual consistency of the dual weighted residual method based on a Newton-GMG framework for steady Euler equations

Jingfeng Wang¹ and Guanghui Hu^{*2}

^{1,2}Department of Mathematics, University of Macau.

²Zhuhai UM Science and Technology Research Institute, Zhuhai, Guangdong, China.

³Guangdong-Hong Kong-Macao Joint Laboratory for Data-Driven Fluid Mechanics and Engineering Applications, University of Macau, China.

March 15, 2023

Abstract

The dual consistency, which is an important issue in developing dual-weighted residual error estimation towards the goal-oriented mesh adaptivity, is studied in this paper both theoretically and numerically. Based on the Newton-GMG solver, dual consistency has been discussed in detail to solve the steady Euler equations. Theoretically, based on the Petrov-Galerkin method, the primal and dual problems, as well as the dual consistency, are deeply studied. It is found that dual consistency is important both for error estimation and stable convergence rate for the quantity of interest. Numerically, through the boundary modification technique, dual consistency can be guaranteed for the problem with general configuration. The features of the proposed dual-consistent DWR-based h -adaptivity on Newton-GMG solver include that i). a stable convergence of quantity of interest can be observed from our numerical experiments, ii). an order of magnitude savings of mesh grids can be expected for calculating the quantity of interest compared with the dual-inconsistent implementation.

Keywords— Newton-GMG; DWR-based adaptation; Dual consistency; h -adaptivity; Steady Euler equations

1 Introduction

Mesh adaptation is one of the most important steps to solve a computational fluid dynamics problem. Pointed by [34], mesh generation and adaptivity continue to be significant bottlenecks in the CFD workflow. In order to obtain an economical mesh, developing a good criterion for adaptation is of major concern.

There have been many mature methods in the development of the DWR-based h -adaptivity. As pointed out by [6], adjoint-based techniques have become more widely used in recent years as they have more solid theoretical foundations for error estimation and control analysis. From these theoretical analyses, it is realized that the adjoint consistency property is of vital importance to guarantee error estimation as well as convergence behavior. In [28], the dual consistency is firstly analyzed, showing that the dual-weighted residual framework based on a dual-inconsistent mesh adaptation may lead to dual solutions with oscillations. Nevertheless, the adjoint consistency is not usually satisfied under certain issues, which results from the mismatch between the quantity of interest and the boundary conditions. In order to address this issue, the modification to the numerical schemes shall be realized. Then, Hartmann proposed a series of boundary modification techniques [13] to extend the analysis to general configurations.

In order to derive a dual-consistent framework, compatibility and consistency should be discussed accordingly. Firstly, compatibility puts emphasis on the dual part, whereby the quantity of interest generated by the functional of dual solutions should theoretically be equal to that of the primal solutions. Giles utilized a matrix representation approach to derive a continuous version of dual equations of Euler equations with different kinds of boundary conditions [7]. However, under certain boundary conditions, dual equations show be equipped with non-trivial strong boundary conditions to ensure the dual consistency. To facilitate the implementation of the DWR method in a discretized finite volume scheme, Darmofal developed a fully discrete method, which is easier to be implemented. Secondly, the consistency part highlights the importance of the discretization method. Analysis of the discontinuous Galerkin scheme by [12][28] has shown that dual consistency requires specific prerequisites to be met in the discretization process. As highlighted by [14], the main reason for the dual inconsistency is the impact of summation by part, underscoring the importance of careful discretization. Moreover, to apply the method for hp -adaptation, Vít Dolejší et al. have developed algorithms for solving the adjoint-based problems [33], which have been applied to the Euler equations in [5].

In our previous work, a Newton-GMG framework has been well-developed for solutions of steady Euler equations. Euler equations are essential for shape optimal design of vehicles and aircraft. However, it may be challenging to develop an efficient and robust iterative solver for nonlinear equations, especially on unstructured meshes. Remarkable progress has been achieved since Jameson [19][22][21] developed numerous numerical techniques for this framework. A homotopy

*Corresponding author(s). E-mail(s): garyhu@um.edu.mo;

method has been applied to solve the steady-state problems of hyperbolic conservation laws since its introduction in [10]. In [25], Li et al. proposed a finite volume solver for 2D steady Euler equations, where the block lower-upper symmetric Gauss-Seidel iteration was implemented as a solver in each Newton iteration. However, developing a robust and efficient solver for nonlinear equations with various configurations is a challenging task. To enhance the robustness of the solver for steady Euler equations, Hu et al.[16] used a WENO-type reconstruction. This approach enables accurate approximation in smooth regions as well as non-oscillatory sharp profiles in the vicinity of shock discontinuities. Additionally, the solver incorporates the Non-Uniform Rational B-Splines (NURBS) method [30][29] for airfoil geometry construction. It is noteworthy that with a series of customized numerical methods, the solver can resolve the system with residual converge to machine precision.

Even though the Newton-GMG solver is effective and robust in solving the steady Euler equations, it still encounters challenges when applying the h -adaptive refinement. The difficulties originate from the theory to derive a well-defined dual equation, the algorithm to obtain dual solutions, and the oscillations in the error of target functions which influence the design of the stop criterion of the algorithm. While the dual-weighted residual method was previously utilized for adaptation in our studies, it is important to note that failure to account for dual consistency may result in unforeseen phenomena. For example, we may obtain unstable convergence curves of the solutions to the dual equations. Besides, the quantity of interest may be even worse when the h -adaptivity is processed. Moreover, the tolerance we adopted in previous work is a constant, which is not efficient in executing the refinement process. Given these challenges, it is crucial to consider the dual consistency property. However, research on the combination of dual consistency and the Newton-GMG solver is presently limited due to the complexity of algorithmic development for the solver and the necessity to explore the preservation of dual consistency within the framework of the Newton-GMG solver.

In this paper, a competitive DWR-based h -adaptive Newton-GMG framework is developed and analyzed towards the dual-consistent property. To resolve the issues mentioned above, dual consistency has been studied thoroughly, and the solver for the dual equations has been further constructed.

For the purpose of developing the DWR-based h -adaptivity method within a dual-consistent framework, both theoretical analyses and algorithm implementation should be studied in depth accordingly. For the theoretical parts, the continuous adjoint and discontinuous Galerkin scheme adjoint methods are reviewed. However, previous studies about the dual consistency and generalized boundary modification method are conducted on a discontinuous Galerkin scheme. Additionally, a k -exact reconstruction framework is considered in this paper, which further complicates the implementation. To tackle these challenges, we use the Petrov-Galerkin method in our finite volume framework to combine the discontinuous Galerkin scheme with our analysis. To ensure that the continuous limit of the dual-consistent framework equals the continuous dual equations exactly, we have to derive a strong form of continuous dual equations. The derivation of such an equation is not trivial due to the nonhomogeneity of physical boundary conditions. Then we reviewed the classical theory to make an analysis. For the algorithm aspect, the basic dual consistency property shall preserve certain restrictions, such as the zero normal velocity condition. Therefore, the boundary modification method proposed by Hartmann is implemented in the framework to develop the algorithm with various boundary conditions. In[5][12], an analysis of different numerical fluxes has been conducted to derive the dual consistency. To ensure the integrity of the Fréchet derivative assumption, the framework is constructed by enforcing the preservation of the first-order derivative. To this end, the numerical fluxes developed in this framework are Lax-Friedrichs and Vijayasundaram schemes. Similar to the modification to the primal equations, regularization terms have been considered to derive the solver for dual equations. For the purpose of enhancing the efficiency of DWR-based h -adaptivity, in the present work, we incorporated the decreasing threshold technique. Moreover, we have made a series of modifications to the entire system, including nonlinear solutions update, geometry generation, and far-field boundary correction. With all these foundations, a highly efficient Godunov scheme can be implemented. In this work, the algorithm has been realized in the library AFVM4CFD developed by our group.

Based on our dual-consistent DWR method, the following three salient features can be observed from a number of numerical experiments. i). The dual equations can be solved smoothly with residuals approaching machine accuracy. ii). A stable convergence of quantity of interest can be guaranteed with the dual consistency. iii). The dual-consistent approach leads to a significant reduction in the number of mesh grids required, as compared to the dual-inconsistent counterpart. The ensuing particulars are as follows. The dual equations are solved with a stable convergence rate, showing that dual consistency is well addressed since a dual-inconsistent framework may lead to dual equations with a lack of regularity. Besides, the solver is tested on a problem involving multiple airfoils, and the results demonstrate that the dual equations focus on the expected area of interest. Moreover, the refinement strategy within a dual-consistent scheme leads to a more accurate quantity of interest with increased degrees of freedom, which is not guaranteed and can be even worse for specific circumstances under a dual-inconsistent framework. Finally, the dual-consistent DWR-based h -adaptivity method helps us save the degree of freedom while a dual-inconsistent case cannot. The results of our study suggest that the DWR method should be implemented under a dual-consistent scheme in the Newton-GMG framework to achieve optimal performance.

The rest of this paper is organized as follows. In Section 1, we present the fundamental notations and provide a concise introduction to the Newton-GMG solver. In Section 2, a brief review of the Newton-GMG solver is given. In Section 3, we discuss the main theory for dual consistency, starting from a continuous dual theory and leading to a dual consistency approach based on the discontinuous Galerkin scheme. As the proposed framework is based on a finite volume scheme, we combine it with the discontinuous Galerkin scheme through Petrov Galerkin analysis. Section 4 is dedicated to the posterior error estimate, where we demonstrate the adjoint consistency of the quantity of interest with the discretization. In Sections 5 and 6, we provide detailed information regarding the algorithm and the discovery of the

combination between adjoint consistency and the Newton-GMG solver.

2 Steady Euler equations

2.1 Basic notations and finite volume method

We begin with some basic notations. Let Ω be a domain in \mathbb{R}^2 with boundary Γ and \mathcal{K}_h be a shape regular subdivision of Ω into different control volumes, K . K_i is used to define the i -th element in this subdivision. $e_{i,j}$ denotes the common edge of K_i and K_j , i.e., $e_{i,j} = \partial K_i \cap \partial K_j$. The unit outer normal vector on the edge $e_{i,j}$ with respect to K_i is represented as $n_{i,j}$. Then \mathcal{V}^{B_h} is the broken function space with cell size h defined on K which contains discontinuous piecewise H^s functions, i.e.,

$$\mathcal{V}^{B_h} = \{v : v|_K \in H^s(K)\}.$$

Similarly, we use $\mathcal{V}_p^{B_h}$ to denote the finite-dimensional spaces on \mathcal{K} with discontinuous piecewise polynomial functions of degree p ,

$$\mathcal{V}_p^{B_h} = \{v : v|_K \in \mathcal{P}_p(K)\},$$

where $\mathcal{P}_p(K)$ is the space of polynomials whose degree $\leq p$ defined on element K with size h . In each control volume $K \in \mathcal{K}_h$, we use \mathbf{u}^+ and \mathbf{u}^- to denote the interior and exterior traces of \mathbf{u} , respectively.

Besides, the flux function $\mathcal{F}(\mathbf{u}) = (\mathbf{f}_1(\mathbf{u}), \mathbf{f}_2(\mathbf{u}))$ is introduced. Then, we can write the conservation law in a compact form: Find $\mathbf{u} : \Omega \rightarrow \mathbb{R}^4$ such that

$$\nabla \cdot \mathcal{F}(\mathbf{u}) = 0, \quad \text{in } \Omega, \quad (2.1)$$

subject to a certain set of boundary conditions.

For the inviscid two-dimensional steady Euler equations, the conservative variable flux is given by

$$\mathbf{u} = \begin{bmatrix} \rho \\ \rho u_x \\ \rho u_y \\ E \end{bmatrix}, \quad \text{and } \mathcal{F}(\mathbf{u}) = \begin{bmatrix} \rho u_x & \rho u_y \\ \rho u_x^2 + p & \rho u_x u_y \\ \rho u_x u_y & \rho u_y^2 + p \\ u_x(E + p) & u_y(E + p) \end{bmatrix}, \quad (2.2)$$

where $(u_x, u_y)^T, \rho, p, E$ denote the velocity, density, pressure and total energy, respectively. In order to close the system in this paper, we use the equation of state

$$E = \frac{p}{\gamma - 1} + \frac{1}{2}\rho(u_x^2 + u_y^2), \quad (2.3)$$

where $\gamma = 1.4$ is the ratio of the specific heat of the perfect gas.

2.2 Petrov Galerkin method

In [18], a high-order adaptive finite volume method is proposed to solve (2.1). As the discretization is conducted under the schemes of the finite volume method, the Euler equations (2.1) are actually solved by the equations reformulated as

$$\mathcal{A}(\mathbf{u}) = \int_{\Omega} \nabla \cdot \mathcal{F}(\mathbf{u}) dx = \sum_i \int_{K_i} \nabla \cdot \mathcal{F}(\mathbf{u}) dx = \sum_i \sum_j \oint_{e_{i,j} \in \partial K_i} \mathcal{F}(\mathbf{u}) \cdot n_{i,j} ds = 0 \quad (2.4)$$

by the divergence theorem. With the numerical flux \mathcal{H} introduced to this scheme, the equations are actually a fully discretized system

$$\sum_i \sum_j \oint_{e_{i,j} \in \partial K_i} \mathcal{H}(\mathbf{u}_i, \mathbf{u}_j) \cdot n_{i,j} ds = 0. \quad (2.5)$$

Here \mathbf{u}_i is the restriction of \mathbf{u} on K_i .

To make a further discussion about the dual-weighted residual method, we need to consider both the error estimates and a higher-order reconstruction of the solution. We adopt the Petrov-Galerkin variant of the discontinuous Galerkin method like in [2], using R_p^0 to denote a reconstruction operator $R_p^0 : \mathcal{V}_0^{B_h} \mapsto \mathcal{V}_p^{B_h}$ which satisfies the cell-averaging condition for $\mathbf{u}_0 \in \mathcal{V}_0^{B_h}$ and $K_i \in \mathcal{K}_h$, i.e.,

$$(R_p^0 \mathbf{u}_0, v)|_{K_i} = (\mathbf{u}_0, v)|_{K_i} = (\mathbf{u}_{0,i}, v), \quad \forall v \in \mathcal{V}_0^{B_h}. \quad (2.6)$$

Here we use (\cdot, \cdot) to denote the L_2 inner product of integration, while $(\cdot, \cdot)|_K$ is the inner product restricted on the control volume K .

With the Petrov Galerkin representation(2.6), the primal control function(2.1) can be reformulated as a weak form in each element,

$$-\int_K \mathcal{F}(R_p^0 \mathbf{u}_0) \cdot \nabla v dx + \int_{\partial K} \mathcal{F}(R_p^0 \mathbf{u}_0^+) \cdot n_K v^+ dx = 0. \quad (2.7)$$

Meanwhile, since \mathbf{u}_0 may be discontinuous between element interfaces, we replace the numerical flux $\mathcal{F}(R_p^0 \mathbf{u}_0^+) \cdot n_K$ with function $\mathcal{H}(R_p^0 \mathbf{u}_0^+, R_p^0 \mathbf{u}_0^-, n_K)$, which depends on both the interior as well as the exterior part of K and the normal

outward vector with respect to K . While the numerical flux on the real boundary Γ does not have an exterior trace, we denote it as $\tilde{\mathcal{H}}(R_p^0 \mathbf{u}_0^+, \Gamma(R_p^0 \mathbf{u}_0^+), n_K)$, where only the interior impact on the boundary Γ has been considered. Then, summing the equation in each control volume, we get *Petrov-Galerkin form discretized Euler equations*:

Find $\mathbf{u}_0 \in \mathcal{V}_0^B$ s.t.

$$\begin{aligned} \mathcal{A}_h(\cdot, \cdot) &:= \sum_{K \in \mathcal{K}_h} \left\{ - \int_K \mathcal{F}(R_p^0 \mathbf{u}_0) \cdot \nabla v dx + \int_{\partial K \setminus \Gamma} \mathcal{H}(R_p^0 \mathbf{u}_0^+, R_p^0 \mathbf{u}_0^-, n_K) v^+ + \int_{\partial K \cap \Gamma} \tilde{\mathcal{H}}(R_p^0 \mathbf{u}_0^+, \Gamma(R_p^0 \mathbf{u}_0^+), n_K) v^+ \right\} \\ &= \sum_{K \in \mathcal{K}_h} \left\{ \int_{\partial K \setminus \Gamma} \mathcal{H}(R_p^0 \mathbf{u}_0^+, R_p^0 \mathbf{u}_0^-, n_K) v^+ + \int_{\partial K \cap \Gamma} \tilde{\mathcal{H}}(R_p^0 \mathbf{u}_0^+, \Gamma(R_p^0 \mathbf{u}_0^+), n_K) v^+ \right\} = 0, \quad \forall v \in \mathcal{V}_0^B. \end{aligned} \quad (2.8)$$

Generally, we denote $\mathcal{J}(\cdot) : \mathcal{V} \rightarrow \mathbb{R}$ as the quantity of interest,

$$\mathcal{J}(\mathbf{u}) = \int_{\Omega} j_{\Omega}(u) dx + \int_{\Gamma} j_{\Gamma}(C u) ds, \quad (2.9)$$

where C is a differential operator. Similarly, the weak form of the quantity of interest can be reformulated as

$$\mathcal{J}(\cdot, \cdot) = \int_{\Omega} j_{\Omega}(R_p^0 \mathbf{u}_0) v dx + \int_{\Gamma} j_{\Gamma}(C(R_p^0 \mathbf{u}_0)) v ds. \quad (2.10)$$

Since the quantity of interest is of central concern in this work, we focus on the theory of solving it via the dual-weighted residual method in the upcoming section.

2.3 Linearization

To solve the equation (3.31), we utilize the Newton iteration method by expanding the nonlinear term through a Taylor series and neglecting the higher-order terms. Then we get

$$\begin{aligned} \sum_i \sum_j \int_{e_{i,j} \in \partial \mathcal{K}_i} \mathcal{H}(\mathbf{u}_i^{(n)}, \mathbf{u}_j^{(n)}) \cdot n_{i,j} ds + \sum_i \sum_j \int_{e_{i,j} \in \partial \mathcal{K}_i} \Delta \mathbf{u}_i^{(n)} \frac{\partial \mathcal{H}(\mathbf{u}_i^{(n)}, \mathbf{u}_j^{(n)})}{\partial \mathbf{u}_i^{(n)}} \cdot n_{i,j} ds \\ + \sum_i \sum_j \int_{e_{i,j} \in \partial \mathcal{K}_i} \Delta \mathbf{u}_j^{(n)} \frac{\partial \mathcal{H}(\mathbf{u}_i^{(n)}, \mathbf{u}_j^{(n)})}{\partial \mathbf{u}_j^{(n)}} \cdot n_{i,j} ds = 0, \end{aligned} \quad (2.11)$$

where $\Delta \mathbf{u}_i$ is the increment of the conservative variables in the i -th element. After each Newton iteration, the cell average is updated by $\mathbf{u}_i^{(n+1)} = \mathbf{u}_i^{(n)} + \Delta \mathbf{u}_i^{(n)}$. However, the Jacobian matrix in the Newton iteration will sometimes be singular and cannot be solved. To overcome this issue, the regularization term $\int_{K_i} \Delta \mathbf{u}_i^n / \Delta t_i dx$, which stands for the artificial time derivative term generally, will be added to the system. The artificial local time step is often given as $CFL \times h_{K_i} / (|u| + c)$ where h_{K_i} is the local grid size and c is the speed of sound. While the local residual can quantify whether the solution is close to a steady state, it serves as a regularization term in this equation. Then this approach leads to the system of *Regularized equations*:

$$\begin{aligned} \alpha \left\| \sum_i \sum_j \int_{e_{i,j} \in \partial \mathcal{K}_i} \mathcal{H}(\mathbf{u}_i^{(n)}, \mathbf{u}_j^{(n)}) \cdot n_{i,j} ds \right\|_{L_1} \Delta \mathbf{u}_i^{(n)} + \sum_i \sum_j \int_{e_{i,j} \in \partial \mathcal{K}_i} \Delta \mathbf{u}_i^{(n)} \frac{\partial \mathcal{H}(\mathbf{u}_i^{(n)}, \mathbf{u}_j^{(n)})}{\partial \mathbf{u}_i^{(n)}} \cdot n_{i,j} ds \\ + \sum_i \sum_j \int_{e_{i,j} \in \partial \mathcal{K}_i} \Delta \mathbf{u}_j^{(n)} \frac{\partial \mathcal{H}(\mathbf{u}_i^{(n)}, \mathbf{u}_j^{(n)})}{\partial \mathbf{u}_j^{(n)}} \cdot n_{i,j} ds \\ = - \sum_i \sum_j \int_{e_{i,j} \in \partial \mathcal{K}_i} \mathcal{H}(\mathbf{u}_i^{(n)}, \mathbf{u}_j^{(n)}) \cdot n_{i,j} ds. \end{aligned} \quad (2.12)$$

This approach offers an advantage in that the regularization coefficient, α , does not require adaptive adjustment and can remain fixed. This feature can be explained by the fact that, during the initial stages of the iteration process, the solution is usually far from achieving a steady state. As the solution is updated accordingly, it gradually approaches the final result. Based on empirical observations, the coefficient α should be calibrated in response to changes in the far-field Mach number. Specifically, larger Mach numbers are associated with larger α values, while smaller ones require smaller coefficients. We set α equal to 2 for the subsonic scheme typically.

Solving this system(2.12) on an unstructured mesh is challenging. However, inspired by the effectiveness of the block lower-upper Gauss-Seidel iteration method proposed in [25] for solving the system, the geometric multigrid method with the agglomeration technique is included in our framework. The solver in this work behaves satisfactorily not only on the primal equations but also on the dual equations, which will be discussed later.

3 Dual-Consistency

Generally, the discussion about the dual-consistency, or adjoint-consistency, such as in [12], consists of two parts. The first part concerns the dual part, which should satisfy the compatible condition. And the second part concerns consistency part. There are different methods to derive a well-defined adjoint discrete equation. For example, starting from the primal continuous equation, we can derive an adjoint equation and then discretize this adjoint equation to get the discrete version of the adjoint equation. If this discrete version of the adjoint equation is compatible with the discrete version of the primal equation, we define it as adjoint consistent. Alternatively, we can discretize the primal equation and then find the adjoint equation of this discrete equation. If this adjoint discrete equation is consistent with the adjoint equation of the primal equation, it also satisfies the adjoint consistency. Whether the consistency property holds or not depends on the numerical scheme or discretization method used, whereas the compatible condition is determined by how the adjoint equation is derived. These two properties are discussed in this section accordingly.

Here we use $(\cdot)^*$ to denote the adjoint version of a certain operator. While the \mathcal{A}^* is usually derived with the method of integration by part, our main concern is the relation between \mathcal{B} and \mathcal{B}^* , \mathcal{C} and \mathcal{C}^* . \mathcal{B} is related to the boundary condition, while the \mathcal{C} is mainly determined by the quantity of interest. In work by [7], the method for deriving a well-posed adjoint equation is well discussed, and we follow this theory to formulate the system based on our scheme.

3.1 Continuous Adjoint

The continuous adjoint approach has been a valuable technique for aerospace application and optimal design, which was pioneered by Jameson[20]. For the compatibility part, the dual equations should be derived such that the quantity of interest based on the dual solution theoretically leads to an identical value. Originating from the continuous equation, Giles and Pierce proved that there is a limited set of objective functions for which the standard formulation of the dual problem is well-posed under certain restrictions of the boundary conditions. While the fully discrete adjoint method is widely used due to its ease in generating the adjoint code, the continuous version remains valuable for deriving a compatible dual problem and providing a deeper understanding of the governing equation and associated schemes. The following analysis follows the technique proposed by Giles et al.[7]. The algorithm's implementation requires the calculation of certain values, which we have recalculated.

Definition 1. Compatibility[7]:

To simplify matters, we assume that the primal operators under consideration have already been linearized. Accordingly, we will use a modified notation to differentiate it from the previous discussion.

Then the primal problem is

$$\begin{aligned} \text{Solve the Quantity of Interest:} & \quad J = (\bar{j}_\Omega, u)_\Omega + (\bar{j}_\Gamma, \mathcal{C}u)_\Gamma, \\ \text{Given the p.d.e.} & \quad \mathcal{A}u = l \quad \text{in } \Omega, \\ \text{With the Boundary Condition} & \quad \mathcal{B}u = g \quad \text{on } \Gamma. \end{aligned} \tag{3.1}$$

Subsequently, the adjoint problem is derived as:

$$\begin{aligned} \text{Solve the Quantity of Interest:} & \quad J = (z, l)_\Omega + (\mathcal{C}^*z, g)_\Gamma, \\ \text{Given the p.d.e.} & \quad \mathcal{A}^*z = \bar{j}_\Omega \quad \text{in } \Omega, \\ \text{With the Boundary Condition} & \quad \mathcal{B}^*z = \bar{j}_\Gamma \quad \text{on } \Gamma. \end{aligned} \tag{3.2}$$

To demonstrate the equivalence of the two problems, it is necessary to prove that the quantity of interest for both equations is equivalent.

$$\begin{aligned} J &= (\bar{j}_\Omega, u)_\Omega + (\bar{j}_\Gamma, \mathcal{C}u)_\Gamma = (\mathcal{A}^*z, u)_\Omega + (\mathcal{B}^*z, \mathcal{C}u)_\Gamma, \\ J &= (v, l)_\Omega + (\mathcal{C}^*z, g)_\Gamma = (z, \mathcal{A}u)_\Omega + (\mathcal{C}^*z, \mathcal{B}u)_\Gamma. \end{aligned} \tag{3.3}$$

Since \mathcal{A}^* is based on the integration by part, it is derived from the equation

$$(z, \mathcal{A}u)_\Omega = (\mathcal{A}^*z, u)_\Omega + (\mathcal{A}_1z, \mathcal{A}_2u)_\Gamma. \tag{3.4}$$

To demonstrate the equality of the terms \mathcal{J} in both equations given by (3.3), we must establish the existence of operators \mathcal{B}^* and \mathcal{C}^* such that, given the operators \mathcal{A} , \mathcal{B} , and \mathcal{C} , the following relationship holds.

$$(\mathcal{A}_1z, \mathcal{A}_2u)_\Gamma = (\mathcal{B}^*z, \mathcal{C}u)_\Gamma - (\mathcal{C}^*z, \mathcal{B}u)_\Gamma. \tag{3.5}$$

The truth is that such operators \mathcal{B}^* and \mathcal{C}^* exist and are unique under some restrictions. For example, the non-singular case can be discussed to support the existence of operators. In this case, we use $\mathbf{A}, \mathbf{B}, \mathbf{C}$ to denote the matrices form of the operators $\mathcal{A}, \mathcal{B}, \mathcal{C}$. $\mathbf{q}_1, \mathbf{q}_2$ to denote the vectors containing all the variables of u and z , with the assumption that

$$(\mathcal{A}_1z, \mathcal{A}_2u)_\Omega \equiv \mathbf{q}_2^T \mathbf{M} \mathbf{q}_1. \tag{3.6}$$

If \mathbf{M} is invertible, our objective is to determine the matrices \mathbf{B}^* and \mathbf{C}^* at each boundary point such that

$$\mathbf{M} = (\mathbf{B}^*)^T \mathbf{C} - (\mathbf{C}^*)^T \mathbf{B}. \tag{3.7}$$

We use augmented matrices \mathbf{T} and \mathbf{T}^* to denote

$$\mathbf{T} = \begin{pmatrix} \mathbf{B} \\ \mathbf{C} \end{pmatrix}, \quad \mathbf{T}^* = \begin{pmatrix} -\mathbf{C}^* \\ \mathbf{B}^* \end{pmatrix}. \quad (3.8)$$

Then the equation can be rewritten as

$$\mathbf{M} = (\mathbf{T}^*)^T \mathbf{T}. \quad (3.9)$$

From the equations (3.8) and (3.9), we can obtain \mathbf{B}^* and \mathbf{C}^* . In fact, it can be proven that the well-posedness of the dual problem is equivalent to the well-posedness of the primal problem[9]. However, we have noticed that \mathbf{M} is mainly determined by the specific boundary condition of the problem. For certain types of boundary conditions, such as solid wall conditions with the vanishing normal velocity $\mathbf{n} \cdot (u_x, u_y) = 0$ for the Euler equations, \mathbf{M} may become a singular matrix. In this case, we need to make a variable transformation to use the reduced variables.

In order to analyze the adjoint boundary operator of the Euler equations (2.1), further modifications shall be introduced to handle this nonlinear case. At first, we require the linear form of this equation, where we consider the Fréchet derivative. Herewith,

$$(\nabla \cdot \mathcal{F})(\cdot)'[\mathbf{u}](\tilde{\mathbf{u}}) = \frac{\partial}{\partial x}(\mathbf{f}'_1[\mathbf{u}](\tilde{u})) + \frac{\partial}{\partial y}(\mathbf{f}'_2[\mathbf{u}](\tilde{u})) = 0. \quad (3.10)$$

Returning to the inner product form of the Euler equations and using the integration by part, we will get

$$\left(z, \frac{\partial}{\partial x} \mathbf{f}'_1[\mathbf{u}] \cdot \mathbf{u} + \frac{\partial}{\partial y} \mathbf{f}'_2[\mathbf{u}] \cdot \mathbf{u} \right)_\Omega = (z, M\mathbf{u})_\Gamma + (-\mathbf{f}'_1[\mathbf{u}]^T \frac{\partial z}{\partial x} - \mathbf{f}'_2[\mathbf{u}]^T \frac{\partial z}{\partial y}, \mathbf{u})_\Omega. \quad (3.11)$$

Then M is defined as $n_x \cdot f'_1[u] + n_y \cdot f'_2[u]$.

Here $f'_1[u]$ and $f'_2[u]$ are the Jacobin matrices which are calculated to be

$$f'_1[u] = \begin{bmatrix} 0 & 1 & 0 & 0 \\ \frac{\gamma-3}{2}u_x^2 + \frac{\gamma-1}{2}u_y^2 & (3-\gamma)u_x & (1-\gamma)u_y & \gamma-1 \\ -u_x u_y & u_y & u_x & 0 \\ u_x(\frac{\gamma-1}{2}(u_x^2 + u_y^2) - H) & H - (\gamma-1)u_x^2 & (1-\gamma)u_x u_y & \gamma u_x \end{bmatrix}, \quad (3.12)$$

$$f'_2[u] = \begin{bmatrix} 0 & 0 & 1 & 0 \\ -u_x u_y & u_y & u_x & 0 \\ \frac{\gamma-3}{2}u_y^2 + \frac{\gamma-1}{2}u_x^2 & (1-\gamma)u_x & (3-\gamma)u_y & \gamma-1 \\ u_y(\frac{\gamma-1}{2}(u_x^2 + u_y^2) - H) & (1-\gamma)u_x u_y & H - (\gamma-1)u_y^2 & \gamma u_y \end{bmatrix},$$

where H satisfies

$$\frac{\gamma E}{\rho} = H + \frac{\gamma-1}{2}(u_x^2 + u_y^2).$$

We use $\tilde{u}_n = u_x n_x + u_y n_y$ to denote the normal velocity. Then

$$\mathbf{M} = \begin{bmatrix} 0 & n_x & n_y & 0 \\ \frac{\gamma-1}{2}n_x(u_x^2 + u_y^2) - u_x \tilde{u}_n & (2-\gamma)u_x n_x + \tilde{u}_n & (1-\gamma)u_y n_x + u_x n_y & (\gamma-1)n_x \\ \frac{\gamma-1}{2}n_y(u_x^2 + u_y^2) - u_y \tilde{u}_n & u_y n_x + (1-\gamma)u_x n_y & (2-\gamma)u_y n_y + \tilde{u}_n & (\gamma-1)n_y \\ \frac{\gamma-1}{2}(u_x^2 + u_y^2)\tilde{u}_n - \tilde{u}_n H & H n_x + (1-\gamma)u_x \tilde{u}_n & H n_y + (1-\gamma)u_y \tilde{u}_n & \gamma \tilde{u}_n \end{bmatrix}, \quad (3.13)$$

with eigenvalues

$$\lambda_1 = \tilde{u}_n + c, \quad \lambda_2 = \tilde{u}_n, \quad \lambda_3 = \tilde{u}_n, \quad \lambda_4 = \tilde{u}_n - c, \quad (3.14)$$

and corresponding eigenvectors

$$\alpha_1 = \begin{bmatrix} 1 \\ u_x + c n_x \\ u_y + c n_y \\ H + \tilde{u}_n c \end{bmatrix}, \quad \alpha_2 = \begin{bmatrix} 1 \\ u_x \\ u_y \\ \frac{u_x^2 + u_y^2}{2} \end{bmatrix}, \quad \alpha_3 = \begin{bmatrix} 1 \\ \tilde{u}_n n_x \\ \tilde{u}_n n_y \\ \frac{u_x^2 + u_y^2}{2} - \tilde{u}_n^2 \end{bmatrix}, \quad \alpha_4 = \begin{bmatrix} 1 \\ u_x - c n_x \\ u_y - c n_y \\ H - \tilde{u}_n c \end{bmatrix}. \quad (3.15)$$

Here c is the speed of sound which is given by

$$c = \sqrt{\frac{\gamma p}{\rho}}. \quad (3.16)$$

Furthermore, the vanishing normal velocity boundary condition of the Euler equations is considered in this case, i.e.,

$$\mathcal{B}(\mathbf{u}) = n_x u_x + n_y u_y = 0, \quad \text{on } \Gamma. \quad (3.17)$$

In the research area of the airfoil shape optimal design, lift and drag are two important quantities. So we consider the target functional as

$$\mathcal{J}(\mathbf{u}) = \int_\Gamma j_\Gamma(C\mathbf{u}) ds = \int_\Gamma p_\Gamma(\mathbf{u}) \mathbf{n} \cdot \beta, \quad (3.18)$$

where β in the above formula is given as

$$\beta = \begin{cases} (\cos \alpha, \sin \alpha)^T / C_\infty, & \text{for drag calculation,} \\ (-\sin \alpha, \cos \alpha)^T / C_\infty, & \text{for lift calculation.} \end{cases} \quad (3.19)$$

Here C_∞ is defined as $\frac{1}{2}\gamma p_\infty Ma_\infty^2 l$, where p_∞, Ma_∞, l denote the far-field pressure, far-field Mach number and the chord length of the airfoil, respectively. In the following section, we will demonstrate that the quantity of interest is compatible with the boundary condition (3.17) and the governing equation (2.1). Based on these analyses, the adjoint operator of the adjoint equation is derived.

The matrix \mathbf{M} becomes singular with rank 2 when the normal velocity is 0. To deal with this issue and enable further analysis, we introduce reduced variables. Let $R = (\alpha_1, \alpha_2, \alpha_3, \alpha_4)$, and define $\Lambda = \text{diag}(\lambda_1, \lambda_2, \lambda_3, \lambda_4)$. Then, we can express \mathbf{M} as $\mathbf{M} = R * \Lambda * R^{-1}$. Next, we define a variable transform u_{trans}, z_{trans} such that $(z, \mathcal{A}u)_\Gamma = (z_{trans}, \Lambda u_{trans})_\Gamma$, where

$$\mathbf{u}_{trans} = R^{-1} \mathbf{u} = \begin{bmatrix} \frac{1}{2\gamma\rho} & \frac{\gamma-1}{\gamma}\rho & 0 & \frac{1}{2\gamma\rho} \end{bmatrix}^T. \quad (3.20)$$

We can simplify our calculations by using the reduced vectors $\mathbf{u}_{reduced}$ and $\mathbf{z}_{reduced}$, given by:

$$\mathbf{u}_{reduced} = \begin{bmatrix} u_{trans,1} \\ u_{trans,4} \end{bmatrix}, \quad \mathbf{z}_{reduced} = \begin{bmatrix} z_{trans,1} \\ z_{trans,4} \end{bmatrix}. \quad (3.21)$$

The corresponding reduced diagonal matrix can be expressed as:

$$\Lambda_{reduced} = \begin{bmatrix} c & 0 \\ 0 & -c \end{bmatrix}. \quad (3.22)$$

Due to the nonlinearity of the Euler equations, the following Fréchet derivatives need to be considered in the discussion of the compatibility,

$$\mathcal{B}'[u] = (0, \frac{n_x}{\rho}, \frac{n_y}{\rho}, 0), \quad \mathcal{C}'[u] = p'[u] = (\gamma - 1) \cdot (\frac{u_x^2 + u_y^2}{2}, -u_x, -u_y, 1). \quad (3.23)$$

We can now calculate

$$\mathcal{B}'[u](w) \equiv n_x u_x + n_y u_y = \widetilde{u}_n, \quad \mathcal{C}'[u](w) \equiv p. \quad (3.24)$$

The reduced vectors can be used to obtain the following expressions,

$$\begin{aligned} \mathcal{B}'[u](w) &= \frac{c}{2\rho} \mathbf{u}_{trans,1} + \frac{-c}{2\rho} \mathbf{u}_{trans,4}, \\ \mathcal{C}'[u](w) &= c^2 \mathbf{u}_{trans,1} + c^2 \mathbf{u}_{trans,4}. \end{aligned} \quad (3.25)$$

Substituting these expressions back to the equation, we can calculate:

$$\begin{bmatrix} c & 0 \\ 0 & -c \end{bmatrix} = \begin{bmatrix} -(\mathcal{C}'[u])^{*T} & (\mathcal{B}'[u])^{*T} \end{bmatrix} \cdot \begin{bmatrix} \frac{c}{2\rho} & -\frac{c}{2\rho} \\ \frac{c}{c^2} & \frac{-c}{c^2} \end{bmatrix}. \quad (3.26)$$

Then

$$\begin{aligned} (\mathcal{B}'[u])^*(\mathbf{z}_{trans}) &= \frac{1}{2c} z_{trans,1} - \frac{1}{2c} z_{trans,4}, \\ (\mathcal{C}'[u])^*(\mathbf{z}_{trans}) &= -\rho z_{trans,1} - \rho z_{trans,4}. \end{aligned} \quad (3.27)$$

By putting the variables back to the original variables with the relation $\mathbf{z}_{trans} = R^T z$, we get *continuous dual equations*:

$$-f_1'[u]^T \frac{\partial z}{\partial x} - f_2'[u]^T \frac{\partial z}{\partial y} = 0, \quad (3.28)$$

where the governing equations are obtained from the integration by part(3.11) with boundary conditions,

$$(\mathcal{B}'[u])^* z \equiv n_x z_2 + n_y z_3 = j_\Gamma'[C\mathbf{u}] \equiv \mathbf{n} \cdot \beta. \quad (3.29)$$

Then the quantity of interest is derived as the surface integration of

$$-2\rho \widetilde{u}_n (z_1 + u_x z_2 + u_y z_3 + H z_4). \quad (3.30)$$

Although the adjoint equation has been derived, directly solving it is still challenging due to the lack of a non-trivial boundary equation to restrict the mass matrix. Additionally, since the zero normal velocity condition contains only two characteristics for both the primal and the dual equations, the rank of the mass matrix is reduced to 2 under this circumstance. As a result, the mass matrix for the boundary part may lack regularity, making the use of iteration methods for solving the linear system unstable.

To address this issue, we can derive the discrete equations in a manner similar to (3.31). Herewith,

$$-\sum_i \sum_j \oint_{e_{i,j} \in \partial K_i} F^*(z) \cdot n_{i,j} ds = 0, \quad (3.31)$$

where $F^*(z) = (f'_1[u]^T z, f'_2[u]^T z)$. The regularization method we discussed for the primal Euler equations can also solve this equation, but subject to an inverse time direction.

To overcome the challenge posed by the strong boundary condition, Giles proposed a method in [9] that factorizes the operator into the interior and boundary parts. The main advantage we get from the dual equations is to use the information from the dual solutions to update our mesh rather than calculate the quantity of interest by the dual solutions. Although the dual equations can theoretically derive an identical quantity of interest through the compatibility property, the linearization process can sometimes pollute the adjoint equations, resulting in a less robust result. This critical issue motivates us to discuss the dual consistency theory.

3.2 Fully Discrete Adjoint

As we discussed in [17], the framework proposed by Darmofal[35] developed a fully adjoint weighted residual method which is well applied in the finite volume scheme. The method was later applied to two-dimensional inviscid flows in [36]. To apply this method in our framework, we provide a brief review of the method. The original motivation for this method was to accurately estimate the numerical integral of $J(\mathbf{u})$ on a fine mesh, $J_h(\mathbf{u}_h)$, without computing the solution on the fine mesh. A multiple-variable Taylor series expansion is used to achieve this goal.

$$J_h(\mathbf{u}_h) = J_h(\mathbf{u}_h^H) + \left. \frac{\partial J_h}{\partial \mathbf{u}_h} \right|_{\mathbf{u}_h^H} (\mathbf{u}_h - \mathbf{u}_h^H) + \dots, \quad (3.32)$$

here \mathbf{u}_h^H represents the coarse solution \mathbf{u}_H mapped onto the fine space \mathcal{V}_h via some prolongation operator I_h^H ,

$$\mathbf{u}_h^H = I_h^H \mathbf{u}_H. \quad (3.33)$$

We denote the residual of the primal problem in the space \mathcal{V}_h using the vector form $\mathcal{R}_h(\cdot)$. It is evident that this residual should be zero when evaluated at the solution \mathbf{u}_h , i.e.,

$$\mathcal{R}_h(\mathbf{u}_h) = 0. \quad (3.34)$$

Moreover, upon linearizing this equation, we obtain the equations below,

$$\mathcal{R}_h(\mathbf{u}_h) = \mathcal{R}_h(\mathbf{u}_h^H) + \left. \frac{\partial \mathcal{R}_h}{\partial \mathbf{u}_h} \right|_{\mathbf{u}_h^H} (\mathbf{u}_h - \mathbf{u}_h^H) + \dots \quad (3.35)$$

As $\left. \frac{\partial \mathcal{R}_h}{\partial \mathbf{u}_h} \right|_{\mathbf{u}_h^H}$ is the Jacobin matrix, symbolically, we can invert this matrix to obtain an approximation of the error vector,

$$\mathbf{u} - \mathbf{u}_h^H \approx - \left(\left. \frac{\partial \mathcal{R}_h}{\partial \mathbf{u}_h} \right|_{\mathbf{u}_h^H} \right)^{-1} \mathcal{R}_h(\mathbf{u}_h^H). \quad (3.36)$$

After putting the error vector (3.36) into the residual vector (3.35), we can get

$$J_h(\mathbf{u}_h) = J_h(\mathbf{u}_h^H) - (\mathbf{z}_h|_{\mathbf{u}_h^H})^T \mathcal{R}_h(\mathbf{u}_h^H), \quad (3.37)$$

where $\mathbf{z}_h|_{\mathbf{u}_h^H}$ is obtained from *Fully discrete dual equations*:

$$\left(\left. \frac{\partial \mathcal{R}_h}{\partial \mathbf{u}_h} \right|_{\mathbf{u}_h^H} \right)^T \mathbf{z}_h|_{\mathbf{u}_h^H} = \left(\left. \frac{\partial J_h}{\partial \mathbf{u}_h} \right|_{\mathbf{u}_h^H} \right)^T. \quad (3.38)$$

The equation (3.37) can be used to update the quantity of interest. The second term, also known as the remaining error, can serve as a local error indicator to guide the mesh adaptation. For a higher-order enhancement, an error correction method has been proposed in the general framework in [32]. So as to apply the adjoint correction method to this fully discrete adjoint weighted residual method, the quantity error has been split into two terms,

$$J_h(\mathbf{u}_h) - J_h(\mathbf{u}_h^H) \approx (L_h^H \mathbf{z}_H)^T \mathcal{R}_h(\mathbf{u}_h^H) + (\mathbf{z}_h|_{\mathbf{u}_h^H} - L_h^H \mathbf{z}_H)^T \mathcal{R}_h(\mathbf{u}_h^H), \quad (3.39)$$

where L_h^H is the prolongation operator that projects the adjoint solution from \mathcal{V}_H into \mathcal{V}_h . In order to denote the residual of the adjoint equation, the operator \mathcal{R}_h^z has been introduced as

$$\mathcal{R}_h^z(\mathbf{z}) \equiv \left(\left. \frac{\partial \mathcal{R}_h}{\partial \mathbf{u}_h} \right|_{\mathbf{u}_h^H} \right)^T \mathbf{z} - \left(\left. \frac{\partial J_h}{\partial \mathbf{u}_h} \right|_{\mathbf{u}_h^H} \right)^T. \quad (3.40)$$

From the equation $\mathcal{R}_h^z(\mathbf{z}_h|\mathbf{u}_h^H) = 0$, we can get

$$\mathcal{R}_h^z(L_h^H \mathbf{z}_H) = \left(\frac{\partial \mathcal{R}_h}{\partial \mathbf{u}_h} \Big|_{\mathbf{u}_h^H} \right)^T (L_h^H \mathbf{z}_H - \mathbf{z}_h|\mathbf{u}_h^H). \quad (3.41)$$

With this equation substituted into (3.39), we can get

$$J_h(\mathbf{u}_h) - J_h(\mathbf{u}_h^H) \approx (L_h^H \mathbf{z}_H)^T \mathcal{R}_h(\mathbf{u}_h^H) - \left\{ \mathcal{R}_h^z(\mathbf{z}_h|\mathbf{u}_h^H) \right\}^T \left(\frac{\partial \mathcal{R}_h}{\partial \mathbf{u}_h} \Big|_{\mathbf{u}_h^H} \right)^{-1} \mathcal{R}_h(\mathbf{u}_h^H). \quad (3.42)$$

And this is equivalent to

$$J_h(\mathbf{u}_h) - J_h(\mathbf{u}_h^H) \approx (L_h^H \mathbf{z}_H)^T \mathcal{R}_h(\mathbf{u}_h^H) + \left\{ \mathcal{R}_h^z(\mathbf{z}_h|\mathbf{u}_h^H) \right\}^T (\mathbf{u}_h - \mathbf{u}_h^H). \quad (3.43)$$

The correction term in the equation (3.39) incorporates the residual of the primal problem, while the correction term in the equation (3.43) incorporates the residual of the dual problem. To combine these two equations, we can consider the duality gap between them, which is defined as follows:

$$D \equiv (\mathbf{z}_h|\mathbf{u}_h^H - L_h^H \mathbf{z}_H)^T \mathcal{R}_h(\mathbf{u}_h^H) - \left\{ \mathcal{R}_h^z(\mathbf{z}_h|\mathbf{u}_h^H) \right\}^T (\mathbf{u}_h - \mathbf{u}_h^H). \quad (3.44)$$

In [35], the (3.44) is shown to be equal to $(\mathbf{z}_h|\mathbf{u}_h^H - L_h^H \mathbf{z}_H)^T \cdot \frac{1}{2} (\mathbf{u}_h - \mathbf{u}_h^H)^T \frac{\partial^2 \mathcal{R}_h}{\partial \mathbf{u}_h^2} \Big|_{\mathbf{u}_h^H} (\mathbf{u}_h - \mathbf{u}_h^H)$. While the error correction method introduces additional calculations of the residual of the dual solutions, for the purpose of validating the dual consistency theory in this work, we only considered the algorithm with the first order decreasing.

3.3 Dual Consistency

In the first part of section 3, we reviewed the basic theory for deriving a well-posed continuous dual equation. Dual consistency, or adjoint consistency, is closely related to the smoothness of the discrete dual solutions. If a discretization is implemented under a dual-consistent scheme, the discrete dual solutions should approximate the continuous dual solutions as the refinement level increases. Conversely, a dual-inconsistent scheme may generate dual solutions with unexpected oscillations or exhibit some non smoothness. Hence, in this part, we will discuss the discretization method and validate whether the dual consistency property can be preserved under this scheme.

As discussed above, the finite volume method is adopted in this work with the introduction of the Petrov-Galerkin method. Therefore, we need to perform elaborate analyses to verify dual consistency under the Petrov-Galerkin form finite volume scheme. In [12], Ralf Hartmann developed analyses about adjoint consistency under the discontinuous Galerkin scheme. Motivated by this work, further analyses are made to discuss the dual consistency in this study.

In (2.8), the discretized primal equations are defined as:

Find $\mathbf{u}_0 \in \mathcal{V}_0^{B_h}$, s.t.

$$\mathcal{A}_h(R_p^0 \mathbf{u}_0, v_0) = 0, \quad \forall v_0 \in \mathcal{V}_0^{B_h}. \quad (3.45)$$

Similarly, the continuous version of primal equations can be defined as :

Find $\mathbf{u} \in \mathcal{V}$, s.t.

$$\mathcal{A}(\mathbf{u}, v) = 0, \quad \forall v \in \mathcal{V}. \quad (3.46)$$

Then the continuous exact dual solutions are derived like (3.40):

Find $z \in \mathcal{V}$, s.t.

$$\mathcal{A}'[\mathbf{u}](w, z) + \mathcal{J}'[\mathbf{u}](w) = 0, \quad \forall w \in \mathcal{V}. \quad (3.47)$$

The primal consistency is held when the exact solution \mathbf{u} satisfies the discretized operator:

$$\mathcal{A}_h(\mathbf{u}, v_0) = 0, \quad \forall v_0 \in \mathcal{V}_0^{B_h}. \quad (3.48)$$

The quantity of interest is defined as *dual-consistent*[12] with the governing equations if the discretized operators satisfy:

$$\mathcal{A}'_h[\mathbf{u}](w, z) + \mathcal{J}'_h[\mathbf{u}](w) = 0, \quad \forall w \in \mathcal{V}_p^{B_h}. \quad (3.49)$$

As in (2.8), we defined the discretized operator. By using the Fréchet derivatives, the linearized form is

$$\begin{aligned} \mathcal{A}'_h[R_p^0 \mathbf{u}_0](w, v) = & \sum_{K \in \mathcal{K}_h} \left\{ \int_{\partial K \setminus \Gamma} \mathcal{H}'[R_p^0 \mathbf{u}_0^+](R_p^0 \mathbf{u}_0^+, R_p^0 \mathbf{u}_0^-, n_K) w^+ v_0^+ ds + \int_{\partial K \setminus \Gamma} \mathcal{H}'[R_p^0 \mathbf{u}_0^-](R_p^0 \mathbf{u}_0^+, R_p^0 \mathbf{u}_0^-, n_K) w^- v_0^+ ds \right\} \\ & + \sum_{K \in \mathcal{K}_h} \left\{ \int_{\partial K \cap \Gamma} \tilde{\mathcal{H}}'[R_p^0 \mathbf{u}_0^+](R_p^0 \mathbf{u}_0^+, \Gamma(R_p^0 \mathbf{u}_0^+), n_K) w^+ v_0^+ ds + \int_{\partial K \cap \Gamma} \tilde{\mathcal{H}}'[\Gamma(\cdot)](R_p^0 \mathbf{u}_0^+, \Gamma(R_p^0 \mathbf{u}_0^+), n_K) \Gamma'[R_p^0 \mathbf{u}_0^+] w^+ v_0^+ ds \right\}. \end{aligned} \quad (3.50)$$

The quantity of interest (3.18) is similarly linearized as

$$\mathcal{J}'[R_p^0 \mathbf{u}_0](w) = \sum_{K \in \mathcal{K}_h} \int_{\partial K \cap \Gamma} j'_\Gamma[R_p^0 \mathbf{u}_0](w) ds = \sum_{K \in \mathcal{K}_h} \int_{\partial K \cap \Gamma} p'_\Gamma[R_p^0 \mathbf{u}_0](w) \mathbf{n} \cdot \beta ds. \quad (3.51)$$

As we discussed the numerical dual solutions process in (3.38), then the dual solutions in a residual form are denoted as: Find $\mathbf{z}_0 \in \mathcal{V}_0^{B_h}$, s.t. given $\mathbf{u}_0 \in \mathcal{V}_0^{B_H}$,

$$\sum_{K \in \mathcal{K}_h} \int_{\partial K \setminus \Gamma} w^+ \cdot r^*[R_p^0(\mathbf{u}_0)_h^H](\mathbf{z}_0) ds + \sum_{K \in \mathcal{K}_h} \int_{\partial K \cap \Gamma} w^+ \cdot r_\Gamma^*[R_p^0(\mathbf{u}_0)_h^H](\mathbf{z}_0) ds, \quad \forall w \in \mathcal{V}_0^{B_h}, \quad (3.52)$$

where

$$\begin{aligned} r^*[R_p^0(\mathbf{u}_0)_h^H](\mathbf{z}_0) &= -(\mathcal{H}'[R_p^0(\mathbf{u}_0^+)_h^H](R_p^0(\mathbf{u}_0^+)_h^H, R_p^0(\mathbf{u}_0^-)_h^H, n_K^+))^T \llbracket \mathbf{z}_0 \rrbracket \cdot n_K^+, & \text{on } \partial K \setminus \Gamma, \\ r_\Gamma^*[R_p^0(\mathbf{u}_0)_h^H](\mathbf{z}_0) &= j'_\Gamma[R_p^0(\mathbf{u}_0^+)_h^H](w) - \left(\tilde{\mathcal{H}}'[R_p^0(\mathbf{u}_0^+)_h^H](\cdot) + \tilde{\mathcal{H}}'[\Gamma(\cdot)](\cdot) \Gamma'[R_p^0(\mathbf{u}_0^+)_h^H] \right)^T \mathbf{z}_0^+, & \text{on } \partial K \cap \Gamma. \end{aligned} \quad (3.53)$$

In order to show the adjoint consistency, we need to prove that the equations below are satisfied with the exact primal solutions \mathbf{u} and the exact dual solutions \mathbf{z} .

$$\sum_{K \in \mathcal{K}_h} \int_{\partial K \setminus \Gamma} w^+ \cdot r^*[\mathbf{u}](\mathbf{z}) ds + \sum_{K \in \mathcal{K}_h} \int_{\partial K \cap \Gamma} w^+ \cdot r_\Gamma^*[\mathbf{u}](\mathbf{z}) ds = 0, \quad \forall w \in \mathcal{V}_0^{B_h}. \quad (3.54)$$

As we are considering the solid wall boundary condition with zero normal velocity, the solutions on the boundary should satisfy $(u_\Gamma)_x n_x + (u_\Gamma)_y n_y = 0$. Generally, we can apply the boundary value operator below.

Definition 2. *Boundary modification operator for zero normal velocity*[12]:

$$\Gamma(\mathbf{u}) := \begin{bmatrix} 1 & 0 & 0 & 0 \\ 0 & 1 - n_1^2 & -n_1 n_2 & 0 \\ 0 & -n_1 n_2 & 1 - n_2^2 & 0 \\ 0 & 0 & 0 & 1 \end{bmatrix} \mathbf{u} = \mathbf{u}_\Gamma, \quad \text{on } \Gamma. \quad (3.55)$$

In [12], the authors discuss a specific case where the numerical flux can be expressed as in Equation (3.56).

$$\tilde{\mathcal{H}}(R_p^0(\mathbf{u}_0^+), \Gamma(R_p^0(\mathbf{u}_0^+)), n_K^+) = n_K \cdot \mathcal{F}(\Gamma(R_p^0 \mathbf{u}_0^+)) = (0, n_1 \tilde{p}_\Gamma, n_2 \tilde{p}_\Gamma, 0)^T. \quad (3.56)$$

where \tilde{p}_Γ is the pressure of reconstructed solutions on the boundary. In this case, the numerical flux is only dependent on the interior trace of the boundary. Using this fact, they reformulate the inner part of the quantity of interest as in Equation (3.57).

$$\tilde{p}_\Gamma n_K \cdot \beta = \tilde{\mathcal{H}}(R_p^0(\mathbf{u}_0^+), \Gamma(R_p^0(\mathbf{u}_0^+)), n_K^+) \cdot \tilde{\beta}, \quad (3.57)$$

where $\tilde{\beta}$ is defined as the augmented vector $\tilde{\beta} := (0, \beta_1, \beta_2, 0)^T$. Then the equations $r_\Gamma^*[\mathbf{u}](\mathbf{z}) = 0$ are held on the boundary Γ with exact value \mathbf{u} and \mathbf{z} once the derivative is taken from (3.56). And equations $r^*[\mathbf{u}](\mathbf{z}) = 0$ are held for the inner boundary due to the smoothness property of the dual solutions. However, (3.56) is a sufficient condition for the dual consistency, which may not be suitable for generalized circumstances. For the purpose of ensuring the preservation of the dual consistency property, generalized boundary modification methods are applied, as discussed in [13][5].

If we want to consider the mirror reflection boundary condition, we shall reconsider the boundary operator as

Definition 3. *Boundary modification operator for mirror reflection*[12]:

$$\Gamma_{\mathcal{M}}(\mathbf{u}) := \begin{bmatrix} 1 & 0 & 0 & 0 \\ 0 & 1 - 2n_1^2 & -2n_1 n_2 & 0 \\ 0 & -2n_1 n_2 & 1 - 2n_2^2 & 0 \\ 0 & 0 & 0 & 1 \end{bmatrix} \mathbf{u} = \mathbf{u}_{\Gamma_{\mathcal{M}}}, \quad \text{on } \Gamma. \quad (3.58)$$

In this circumstance, the quantity of interest is dual-consistent with the discretization when the numerical flux on the boundary is defined as $\tilde{\mathcal{H}}(R_p^0(\mathbf{u}_0^+), \Gamma_{\mathcal{M}}(R_p^0(\mathbf{u}_0^+)), n_K^+)$. Consequently, the quantity of interest within a dual-consistent scheme is given by

$$\mathcal{J}(\mathbf{u}) = \int_\Gamma j_{\Gamma_{\mathcal{M}}}(C\mathbf{u}) ds = \int_\Gamma p((\Gamma_{\mathcal{M}}(\mathbf{u})) \mathbf{n} \cdot \beta). \quad (3.59)$$

In [5] and [13], it was shown that certain numerical fluxes, such as Vijayasundaram and Lax-Friedrichs, maintain the dual consistency property. However, other types of nonlinear numerical fluxes may not necessarily preserve the smoothness of dual solutions due to the linearization process involved. In the present work, the Lax-Friedrichs numerical flux was found to perform best for the scheme. Various methods have been discussed in previous literature for linearizing the numerical flux and quantity of interest, including the analytic method, finite difference approximation, complex step method, and algorithmic differentiation [23][24]. Acceleration techniques have also been developed for solving the adjoint problem. In this work, we restrict the validation to a two-dimensional model, and we use the finite difference method due

to its simplicity and fewer memory requirements. The behavior of the solver using the finite difference method met our expectations. The idea can be summed up as an approximation to the analytical derivative, where the Jacobian matrix $\partial\mathcal{R}_i/\partial\mathbf{u}_j$ can be denoted as

$$\frac{\partial\mathcal{R}_i}{\partial\mathbf{u}_j} = \lim_{\epsilon \rightarrow 0} \frac{\mathcal{R}(\dots, \mathbf{u}_j + \epsilon, \dots) - \mathcal{R}(\dots, \mathbf{u}_j, \dots)}{\epsilon} \approx \frac{\mathcal{R}(\dots, \mathbf{u}_j + \epsilon, \dots) - \mathcal{R}(\dots, \mathbf{u}_j, \dots)}{\epsilon}. \quad (3.60)$$

The choice of ϵ is crucial in numerical differentiation as it affects the accuracy and stability of the approximation. If ϵ is too small, numerical errors may dominate, and the calculation can become ill-conditioned, leading to a loss of significance. On the other hand, if ϵ is too large, the approximation may destroy the accuracy of the truncation error. In this work, $\epsilon = \epsilon_0 \mathbf{u}_j$ is adopted, where $\epsilon_0 = 1.0e - 8$ is set in the simulations. This choice of ϵ is similar to that used for the derivative of the quantity of interest $\partial\mathcal{J}_i/\partial\mathbf{u}_j$.

As discussed in [5], a quantity of interest is dual-inconsistent if the integrand is not considered under this dual consistency scheme. For example, we will consider an example of *dual-inconsistent scheme* [5] below.

In this case, the Fréchet directional derivative is given by

$$\mathcal{J}'[R_p^0 \mathbf{u}_0](w) = \sum_{K \in \mathcal{K}_h} \int_{\partial K \cap \Gamma} j'_\Gamma[R_p^0 \mathbf{u}_0](w) \cdot \phi ds, \quad (3.61)$$

where $j'_\Gamma[R_p^0 \mathbf{u}_0](w) \cdot \phi = \lim_{t \rightarrow 0} \frac{1}{t} (j_\Gamma(R_p^0 \mathbf{u}_0 + t\phi) - j_\Gamma(R_p^0 \mathbf{u}_0))$ and ϕ is a small directional perturbation, while $\phi_j = \epsilon_0(R_p^0 \mathbf{u}_j)$

is used to calculate the derivatives on the boundary. And $j'_\Gamma[R_p^0 \mathbf{u}_0](w) = \frac{d\tilde{p}_n}{d\mathbf{u}} \tilde{\beta}$, where

$$\frac{d\tilde{p}_n}{d\mathbf{u}} := n_K \otimes \frac{d\tilde{p}}{\mathbf{u}} = (\gamma - 1) \begin{bmatrix} 0 & 0 & 0 & 0 \\ \frac{1}{2}|\tilde{u}_x^2 + \tilde{u}_y^2|n_x & -\tilde{u}_x n_x & -\tilde{u}_y n_x & n_x \\ \frac{1}{2}|\tilde{u}_x^2 + \tilde{u}_y^2|n_y & -\tilde{u}_x n_y & -\tilde{u}_y n_y & n_y \\ 0 & 0 & 0 & 0 \end{bmatrix}. \quad (3.62)$$

Here $n_K := (0, n_x, n_y, 0)^T$ is similarly the augmented vector of n_K . Dolejál et al. selected the quantity of interest as lift and drag for simulation. However, the calculation of lift is oscillatory even if an anisotropic mesh is developed. Hence, we considered the drag coefficient to validate the algorithm in this research. The results are shown in the numerical results section.

Remark 1. *It is worth noting that when the scheme is derived under a dual-consistent framework, $r_\Gamma^*[\mathbf{u}](\mathbf{z}) = 0$, which is equivalent to $p'_\Gamma[\mathbf{u}](\cdot) \cdot \beta = \left(\tilde{\mathcal{H}}[\mathbf{u}](\cdot)\right)^T \mathbf{z}$. By taking a derivative of (3.56), we obtain $\tilde{\mathcal{H}}[\mathbf{u}](\cdot) = \tilde{n}_K \tilde{p}_\Gamma[\mathbf{u}](\cdot)$. Then $\tilde{n}_K \cdot \mathbf{z} = n_K \cdot \beta$ is precisely equivalent to dual equation (3.29) in continuous version.*

In [8], the mechanism with shock waves was discussed from the perspective of governing equations. Different methods to derive dual equations have their own advantages for mesh adaptation and model calculation. Dual consistency is well known to be a significant property that can influence the performance of h -adaptivity. It was first analyzed in [28], and the result shows that a dual-inconsistent scheme may lead to dual solutions with oscillations. Besides, Collis and Heinkenschloss used the dual-inconsistent scheme for the streamline upwind/Petrov-Galerkin method for linear advection-diffusion to an optimal control problem. The discretized continuous dual equations performed better than the discrete dual equations derived from the discrete primal equations.

Though dual consistency is not trivial to be preserved theoretically, the discretization may still be asymptotically adjoint if equations(3.49) hold when taking the limit $h \rightarrow 0$. Even if the dual consistency is not preserved, additional terms can be added to the discretized equations or the quantity of interest to modify the scheme. As shown in [11], symmetric and nonsymmetric interior penalties have been discussed separately. And the SIPG scheme, which is dual-consistent, leads to a better convergence rate of the quantity of interest. In [5], a dual consistent-based hp -adaptive scheme achieved a better convergence rate. In this study, the dual consistency is implemented under the Newton-GMG solver, and the boundary modification is updated in each step. As the dual-inconsistent scheme may pollute the adaptation around the boundary, some unexpected singularities may occur. Then the dual equations may generate a linear system with a loss of regularization. In order to resolve this issue, a regularization term was added to the dual equations, leading to a GMG solver with a more stable convergence rate and generating the error indicators well.

4 A Posteriori Error estimate

4.1 Posteriori Error Representation

In [17], we developed a non-oscillatory k-exact reconstruction method. Based on this work, we consider the finite volume scheme with the Petrov-Galerkin method to make a posterior error estimate which is pioneered by Becker and Rannacher[?]. Firstly, the numerical solution \mathbf{u}_p denotes the solution solved on a finite-dimensional space $\mathcal{V}_p^{B_h}$, which satisfy the equation

$$\mathcal{A}_h(\mathbf{u}_p, v) = 0, \quad \forall v \in \mathcal{V}_p^{B_h}. \quad (4.1)$$

With the orthogonality property that

$$\mathcal{A}_h(\mathbf{u}_p, v) = \mathcal{A}_h(\mathbf{u}, v), \quad \forall v \in \mathcal{V}_p^{B_h}, \quad (4.2)$$

the exact error representation formula is derived from the following steps[2]:

$$\begin{aligned} \mathcal{J}(\mathbf{u}) - \mathcal{J}(\mathbf{u}_p) &= \int_0^1 \mathcal{J}'[\mathbf{u}](\mathbf{u}_p + (\mathbf{u} - \mathbf{u}_p)\theta) d(\mathbf{u} - \mathbf{u}_p)\theta \\ &= \int_0^1 \mathcal{A}'_h[\mathbf{u}](\mathbf{u}_p + (\mathbf{u} - \mathbf{u}_p)\theta, \mathbf{z}) d(\mathbf{u} - \mathbf{u}_p)\theta \\ &= \mathcal{A}_h(\mathbf{u}, \mathbf{z}) - \mathcal{A}_h(\mathbf{u}_p, \mathbf{z}) \\ &= \mathcal{A}_h(\mathbf{u} - \mathbf{u}_p, \mathbf{z}) - \mathcal{A}_h(\mathbf{u} - \mathbf{u}_p, \pi_P \mathbf{z}) \\ &= \mathcal{A}_h(\mathbf{u}, \mathbf{z} - \pi_P \mathbf{z}) - \mathcal{A}_h(\mathbf{u}_p, \mathbf{z} - \pi_P \mathbf{z}) \\ &= -\mathcal{A}_h(\mathbf{u}_p, \mathbf{z} - \pi_P \mathbf{z}). \end{aligned} \quad (4.3)$$

Here π_p denotes a projection operator that maps the exact function into $\mathcal{V}_p^{B_h}$, and the Fréchet derivatives are just formal calculations. Meanwhile, the residual can be separated into two parts[?]:

$$\begin{aligned} \mathcal{J}(\mathbf{u}) - \mathcal{J}(\mathbf{u}_p) &= \mathcal{A}_h(\mathbf{u} - \mathbf{u}_p, \mathbf{z} - \mathbf{z}_p) \\ &= \sum_{K \in \mathcal{K}_h} \left\{ - \int_K \nabla \mathcal{F}(\mathbf{u} - \mathbf{u}_p) \cdot (\mathbf{z} - \mathbf{z}_p) dx \right. \\ &\quad + \int_{\partial K \setminus \Gamma} (\mathcal{F}(\mathbf{u} - \mathbf{u}_p) \cdot n_K - \mathcal{H}((\mathbf{u} - \mathbf{u}_p)^+, (\mathbf{u} - \mathbf{u}_p)^-, n_K)) \cdot (\mathbf{z} - \mathbf{z}_p)^+ ds \\ &\quad \left. + \int_{\partial K \cap \Gamma} (\mathcal{F}(\mathbf{u} - \mathbf{u}_p) \cdot n_K - \tilde{\mathcal{H}}((\mathbf{u} - \mathbf{u}_p)^+, \Gamma((\mathbf{u} - \mathbf{u}_p)^+), n_K)) \cdot (\mathbf{z} - \mathbf{z}_p)^+ ds \right\} \\ &\leq \sum_{K \in \mathcal{K}_h} \rho_K \omega_K, \end{aligned} \quad (4.4)$$

where ρ_K denotes the residuals and ω_K denote weights, defined by

$$\begin{aligned} \rho_K &:= h_K \|\nabla \mathcal{F}(\mathbf{u} - \mathbf{u}_p)\|_{L_K^2} + h_K^{1/2} \|r_K\|_{L_{\partial K \setminus \Gamma}^2} + h_K^{1/2} \|r_K^*\|_{L_{K \cap \Gamma}^2}, \\ \omega_K &:= \max\{h_K^{-1} \|\mathbf{z} - \mathbf{z}_p\|_{L_K^2}, h_K^{-1/2} \|\mathbf{z} - \mathbf{z}_p\|_{L_{\partial K \setminus \Gamma}^2}, h_K^{-1/2} \|\mathbf{z} - \mathbf{z}_p\|_{L_{\partial K \cap \Gamma}^2}\}. \end{aligned} \quad (4.5)$$

Here r_K and r_K^* are defined by

$$\begin{aligned} r_K &:= \mathcal{F}(\mathbf{u} - \mathbf{u}_p) \cdot n_K - \mathcal{H}((\mathbf{u} - \mathbf{u}_p)^+, (\mathbf{u} - \mathbf{u}_p)^-, n_K), \\ r_K^* &:= \mathcal{F}(\mathbf{u} - \mathbf{u}_p) \cdot n_K - \tilde{\mathcal{H}}((\mathbf{u} - \mathbf{u}_p)^+, \Gamma((\mathbf{u} - \mathbf{u}_p)^+), n_K). \end{aligned} \quad (4.6)$$

According to the local approximation estimates in [3], we have

$$\max\{h_K^{-1} \|\mathbf{z} - \mathbf{z}_p\|_{L_K^2}, h_K^{-1/2} \|\mathbf{z} - \mathbf{z}_p\|_{L_{\partial K \setminus \Gamma}^2}, h_K^{-1/2} \|\mathbf{z} - \mathbf{z}_p\|_{L_{\partial K \cap \Gamma}^2}\} \leq C_{i,K} h_K^{1+r} \|\nabla^{1+r} \mathbf{z}\|_{\tilde{K}}, \quad r \in \{0, 1\}, \quad (4.7)$$

for $\mathbf{z} \in \mathcal{V} \cap H^{1+r}(\Omega)$. For $r = 0$, \tilde{K} is the union of its neighboring patch of K while for $r = 1$, \tilde{K} is K itself. Generally, we do not have an explicit bound for the dual solution \mathbf{z} . The simplest way is to consider $r = 1$, and the estimates for the weights ω_K is to substitute the dual solution \mathbf{z} with the approximate value $\mathbf{z}_h \in \mathcal{W}_h$. Then the expression of weight is given by

$$\omega_K \approx \tilde{\omega}_K := h_K^2 |\nabla_h^2 \mathbf{z}_h(x_K)|, \quad (4.8)$$

where x_K denotes the mid-point of element K . Heuristically, if the numerical solution of the adjoint equation is singular at some point, then the mesh needs to be refined. Even when the primal solution is smooth, which leads to a relatively small residual, the dual weight dominates the tolerance in this scheme. Hence, the most important reason for using the dual-weighted residual method is to refine the mesh more economically under different schemes of the quantity of interest. Our objective is not to solve the numerical solution accurately globally but to solve the target variable with higher accuracy instead. The dual weight determines the allocation of computational resources for solving the quantity of interest with greater accuracy. It is important to note that inequality in (4.4) can be formulated with different kinds of methods. In this work, we concentrate on the following schemes for developing the dual weight based on tolerance.

4.2 Reconstruction scheme

We applied the higher-order reconstruction method to avoid the appearance of Galerkin orthogonality in the error representation. However, in (4.3), the lack of an exact value for \mathbf{u} makes the equation unconvincing because the error is

represented by the expression of \mathbf{u} . We will address these issues in this section. For clarity in the proceeding analysis, we consider the linearized $\mathcal{A}_h[\mathbf{u}](\cdot)$ and derive the dual equation as follows in a weak form to facilitate the error analysis,

$$\mathcal{A}_h(\mathbf{u}, v) - \mathcal{A}_h(\mathbf{u}_p, v) = \int_0^1 \mathcal{A}'_h[\mathbf{u}](\mathbf{u}_p + (\mathbf{u} - \mathbf{u}_p)\theta, v) d(\mathbf{u} - \mathbf{u}_p)\theta. \quad (4.9)$$

Similarly, the quantity of interest should also be considered in a linearization way, which is

$$\mathcal{J}(\mathbf{u}) - \mathcal{J}(\mathbf{u}_p) = \int_0^1 \mathcal{J}'[\mathbf{u}](\mathbf{u}_p + (\mathbf{u} - \mathbf{u}_p)\theta) d(\mathbf{u} - \mathbf{u}_p)\theta. \quad (4.10)$$

If the discretization is implemented within a dual-consistent scheme, the weak form of the dual equation can be solved as: Find $\mathbf{z} \in \mathcal{V}$ such that

$$\mathcal{A}_h(\mathbf{u}, \mathbf{z}) - \mathcal{A}_h(\mathbf{u}_p, \mathbf{z}) = \mathcal{J}(\mathbf{u}) - \mathcal{J}(\mathbf{u}_p). \quad (4.11)$$

Then, we denote R_q^p as a reconstruction operator $R_q^p : \mathcal{V}_p^B \rightarrow \mathcal{V}_q^B$ which generates a cell-wise discontinuous q -th order polynomials from a p -th order one on the broken space B_h .

Then based on the reconstruction, we develop the error representation based on the Godunov FVM case:

$$\begin{aligned} \mathcal{J}(\mathbf{u}) - \mathcal{J}(R_p^0 \mathbf{u}_0) &= \int_0^1 \mathcal{J}'[\mathbf{u}](R_p^0 \mathbf{u}_0 + (\mathbf{u} - R_p^0 \mathbf{u}_0)\theta) d(\mathbf{u} - R_p^0 \mathbf{u}_0)\theta \\ &= \int_0^1 \mathcal{A}'_h[\mathbf{u}](R_p^0 \mathbf{u}_0 + (\mathbf{u} - R_p^0 \mathbf{u}_0)\theta, \mathbf{z}) d(\mathbf{u} - R_p^0 \mathbf{u}_0)\theta \\ &= \mathcal{A}_h(\mathbf{u}, \mathbf{z}) - \mathcal{A}_h(R_p^0 \mathbf{u}_0, \mathbf{z}) \\ &= \mathcal{A}_h(\mathbf{u} - R_p^0 \mathbf{u}_0, \mathbf{z}) - \mathcal{A}_h(\mathbf{u} - R_p^0 \mathbf{u}_0, \pi_p \mathbf{z}) \\ &= \mathcal{A}_h(\mathbf{u}, \mathbf{z} - \pi_0 \mathbf{z}) - \mathcal{A}_h(R_p^0 \mathbf{u}_0, \mathbf{z} - \pi_p \mathbf{z}) \\ &= -\mathcal{A}_h(R_p^0 \mathbf{u}_0, \mathbf{z} - \pi_p \mathbf{z}), \end{aligned} \quad (4.12)$$

where the fourth equation is held by the Galerkin orthogonality

$$\mathcal{A}_h(\mathbf{u}, \pi_p \mathbf{z}) = \mathcal{A}_h(R_p^0 \mathbf{u}_0, \pi_p \mathbf{z}). \quad (4.13)$$

Then the error representation here can be reformulated as the following expression,

$$\begin{aligned} \mathcal{J}(\mathbf{u}) - \mathcal{J}(R_p^0 \mathbf{u}_0) &= \sum_{K \in \mathcal{K}_h} \left\{ - \int_K \nabla \mathcal{F}(R_p^0 \mathbf{u}_0) \cdot (\mathbf{z} - \pi_p \mathbf{z}) dx \right. \\ &\quad + \int_{\partial K \setminus \Gamma} (\mathcal{F}(R_p^0 \mathbf{u}_0^+) \cdot n_K - \mathcal{H}(R_p^0 \mathbf{u}_0^+, R_p^0 \mathbf{u}_0^-, n_K)) \cdot (\mathbf{z} - \pi_p \mathbf{z})^+ ds \\ &\quad \left. + \int_{\partial K \cap \Gamma} (\mathcal{F}(R_p^0 \mathbf{u}_0^+) \cdot n_K - \tilde{\mathcal{H}}(R_p^0 \mathbf{u}_0^+, \Gamma(R_p^0 \mathbf{u}_0^+), n_K)) \cdot (\mathbf{z} - \pi_p \mathbf{z})^+ ds \right\}. \end{aligned} \quad (4.14)$$

However, this representation is not suitable for obtaining a computational posterior error estimate. The reason is that the \mathbf{z} in the formula (4.14) is on the infinite-dimensional space, which is not generally known. Meanwhile, the mean-value linearization used in the error estimates is based on the exact solution of \mathbf{u} , which contradicts the goal of calculating the numerical solution using this scheme.

To approximate the exact value of \mathbf{z} on the infinite-dimensional space, we follow the patch recovery post-processing and global higher-order solves methods in [2]. We substitute an approximation solution \mathbf{z}_0 to the dual equation. Then we use the k-exact reconstruction method used in [17]. This lead to the following problem: Find $\mathbf{z}_0 \in \mathcal{V}_0^{B_h}$ such that

$$\mathcal{A}_h(\mathbf{u}, R_p^0 \mathbf{z}_0) - \mathcal{A}_h(\mathbf{u}_p, R_p^0 \mathbf{z}_0) = \mathcal{J}(\mathbf{u}) - \mathcal{J}(\mathbf{u}_p). \quad (4.15)$$

Then the dual solution on the infinite space can be approximated by $\bar{R}_q^p R_p^0 \mathbf{z}_0$ where \bar{R}_q^p denotes the k-exact reconstruction operator.

Then we use a higher-order reconstruction to substitute the exact value. After that, we solve the primal equation roughly to get \mathbf{u}_0 , which converts the equation into the form: Find $\mathbf{z}_0 \in \mathcal{V}_0^{B_h}$ such that for $q > p$

$$\mathcal{A}_h(R_p^0 \mathbf{u}_0, R_q^0 \mathbf{z}_0) - \mathcal{A}_h(R_q^0 \mathbf{u}_0, R_q^0 \mathbf{z}_0) = \mathcal{J}(R_p^0 \mathbf{u}_0) - \mathcal{J}(R_q^0 \mathbf{u}_0). \quad (4.16)$$

Then the error representation can be formulated as

$$\begin{aligned} Error &= \sum_{K \in \mathcal{K}_h} \mathcal{E}_K \\ &= \sum_{K \in \mathcal{K}_h} \left\{ - \int_K \nabla [R_q^0 \mathbf{u}_0] \mathcal{F}(R_q^0 \mathbf{u}_0) \cdot (R_q^0 \mathbf{z}_0 - \mathbf{z}_0) dx \right. \\ &\quad + \int_{\partial K \setminus \Gamma} (\mathcal{F}(R_q^0 \mathbf{u}_0^+) \cdot n_K - \mathcal{H}(R_q^0 \mathbf{u}_0^+, R_q^0 \mathbf{u}_0^-, n_K)) \cdot (R_q^0 \mathbf{z}_0 - \mathbf{z}_0)^+ ds \\ &\quad \left. + \int_{\partial K \cap \Gamma} (\mathcal{F}(R_q^0 \mathbf{u}_0^+) \cdot n_K - \tilde{\mathcal{H}}(R_q^0 \mathbf{u}_0^+, \Gamma(R_q^0 \mathbf{u}_0^+), n_K)) \cdot (R_q^0 \mathbf{z}_0 - \mathbf{z}_0)^+ ds \right\}. \end{aligned} \quad (4.17)$$

While the whole adaptation scheme is implemented under the Petrov-Galerkin method, it is not possible to calculate dual solutions on a functional space that is the same as the primal solutions due to the potential influence of Galerkin orthogonality on the adaptation, resulting in an error representation of zero.

Various techniques have been proposed to prevent unexpected phenomena resulting from Galerkin orthogonality. These include modifying the size of the broken space and improving the order of piecewise polynomials. For example, a reconstruction method was combined with the goal-oriented method to solve a linear-convection-diffusion-reaction problem in [4]. In our previous work[29][16], the reconstruction method conducted under [37] [26] is efficient, which accelerates the convergence of the system towards the steady state significantly. As a robustness reconstruction had been achieved effectively and the motivation to avoid the Galerkin orthogonality for a theoretical guarantee, the reconstruction method is applied in this research to construct the algorithm framework. Moreover, for further implementation of the reconstruction around the shock waves, we could consider the shock capturing method[27].

5 Numerical Algorithm

5.1 AFVM4CFD

In [34], a comprehensive review of the development of computational fluid dynamics in the past, as well as the perspective in the future 15 years has been delivered, in which the mesh adaptivity was listed as a potential technique for significantly enhancing the simulation efficiency. However, it was also mentioned that such a potential method has not seen widespread use, “due to issues related to software complexity, inadequate error estimation capabilities, and complex geometry”.

In this library, we provide a competitive solution to resolve the above three issues in developing adaptive mesh methods for steady Euler equations through 1). a thorough investigation of the dual consistency in dual-weighted residual methods, 2). a well design of a dual-weighted residual based h -adaptive mesh method with dual consistency, based on a Newton-GMG numerical framework, and 3). a quality code based on AFVM4CFD library. It is worth mentioning that with the AFVM4CFD, the Euler equations can be solved well with a satisfactory residual that gets close to the machine precision. Now AFVM4CFD is under the application of software copyright.

5.2 Newton-GMG for dual equations

In our previous work, the Newton-GMG solver is effective for solving equations. However, the linear system may be ill-posed since the dual-inconsistent framework may cause unexpected singularities around the boundary domain. Therefore, the robustness of the linear system solver is also crucial for the framework. Additionally, the dual equations derived from the primal equations have an inverse direction of time direction based on the integration by part. Then the time term should also be considered in the regularization of the dual linear system. The performance of the solver for the dual equations is shown below:

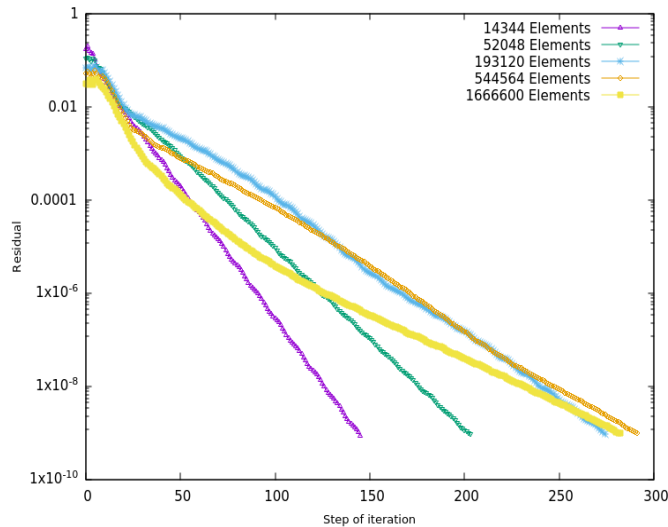


Figure 1: Convergence curves of the residual of dual equations.

As is shown in Figure.1, the solver for dual equations is steady and powerful. Even for the mesh with more than 1,500,000 elements, the convergence trace of the solver is smooth, which supports the whole algorithm of the DWR refinement.

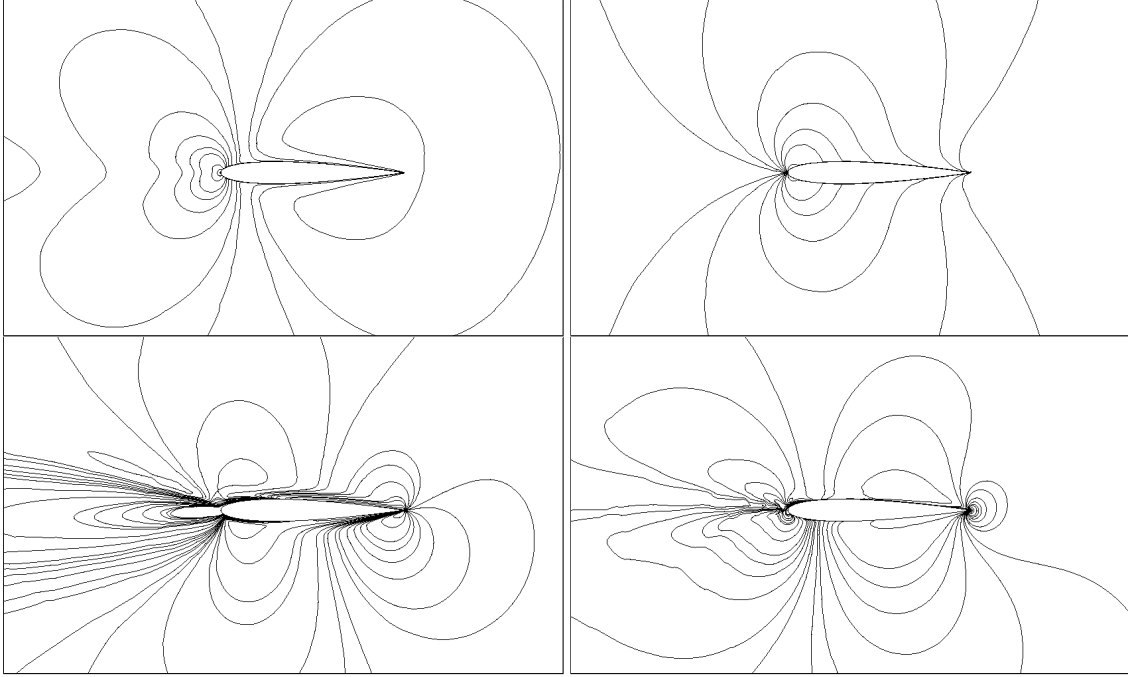


Figure 2: Top: the isolines of the first and second dual momentum variables, with Dual-Consistent DWR method. Bottom: isolines with Dual-Inconsistent DWR method, respectively.

5.3 h -adaptivity Process

From the theoretical discussion above, we developed the DWR-based h -adaptive refinement with a Newton-GMG solver, which solved the equations well. The process for a one-step refinement can be summed up as the algorithm below:

Algorithm 1: DWR for one-step mesh refinement

Data: Initial \mathcal{K}_H, TOL

Result: \mathcal{K}_h

Using the Newton-GMG to solve $\mathcal{R}_H(\mathbf{u}_0) = 0$ with residual tolerance $1.0e - 3$;

Reconstruct the piecewise constant solutions $\mathbf{u}_1 = R_1^0 \mathbf{u}_0$;

Interpolate solution $(\mathbf{u}_1)_H$ from the mesh \mathcal{K}_H to \mathcal{K}_h to get $(\mathbf{u}_1)_h^H$;

Record the residual $\mathcal{R}_h((\mathbf{u}_1)_h^H)$;

Solve the dual equation to get $(\mathbf{z}_0)_H$;

Calculate the error indicator for each element;

while $\mathcal{E}_{\mathcal{K}_H} > TOL$ **for some** \mathcal{K}_H **do**

 | Adaptively refinement the mesh \mathcal{K}_H with the process in [18];

end

In our previous work[18][15], we used a constant tolerance for successive refinements process. However, as the desired precision of the quantity of interest increases, the number of elements in the mesh grows rapidly. Choosing an optimal tolerance is tricky due to the reason that excessive refinement may need too much degree of freedom while inadequate refinement will cause too many steps for refinement and even lead to a significant error result. It has been suggested by [1] that tolerance shall match the error distribution histograms on hierarchical meshes. Besides, Nemec developed a decreasing threshold strategy based on the adjoint-based framework[31], which can help save degrees of freedom for a specific quantity of interest. Motivated by this idea, we have designed the algorithm with a decreasing refinement threshold, and the growth of grids has met expectations well.

6 Numerical experiment

6.1 Subsonic Model

To validate the efficiency of the algorithm, we tested the model with the following configurations:

- A domain with a NACA0012 airfoil, surrounding by an outer circle with a radius of 40;
- Mach number 0.5, and attack angle 0° ;
- Lax-Friedrichs Numerical Flux;
- Drag coefficient as the quantity of interest, and zero normal velocity as the solid wall boundary condition;

To compare the differences between dual consistency and dual inconsistency, we calculate the dual solutions using a mesh with four times global refinement. The drag coefficient can be chosen as the quantity of interest with zero normal velocity boundary conditions, resulting in no normal pressure on the airfoil boundary and a drag coefficient close to 0, i.e., $\mathcal{J}(\mathbf{u}) = 0$. As shown in Figure. 2, the DWR method constructed on a dual-consistent framework generates symmetric and smooth dual solutions, while the dual solutions from the dual-inconsistent framework are oscillatory. This evidence demonstrates that the main difference between these two schemes is the impact on the dual solutions.

The whole algorithm works well when the dual solutions part is included in the calculation. The results of the convergence trace are shown in Figure.3.

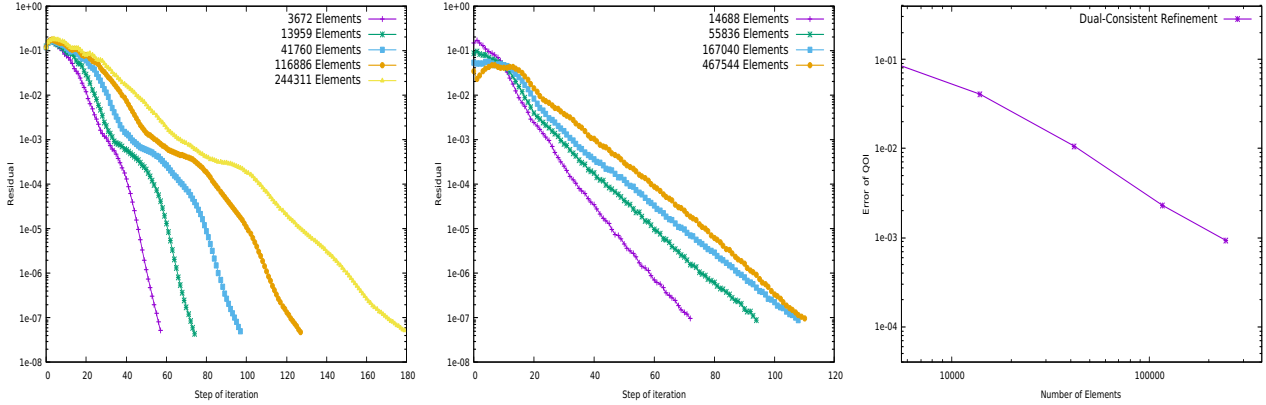


Figure 3: Convergence curves of Newton-GMG solver for the steady Euler equations with successive h -adaptivity. Left: the residual of primal equations; Middle: the residual of dual equations; Right: the error of quantity of interest.

Then, a dual-consistent DWR-based h -adaptivity algorithm is constructed in this framework. Further discussions about dual consistency are conducted based on this solver, and the results are shown with the following simulations.

6.2 Transonic Model

- A domain with a NACA0012 airfoil, surrounding by an outer circle with a radius of 30;
- Mach number 0.8, and attack angle 0° ;
- Lax-Friedrichs Numerical Flux;
- Drag coefficient as the quantity of interest, and mirror reflection as the solid wall boundary condition;

Since the solver for the primal equations is so effective that the residual of equations can converge to machine precision, we use a globally refined mesh with 3672064 elements to calculate the quantity of interest, which is $C_d = 0.00942314$. Then we compared this with the same configurations but with a change in the dual consistency scheme, which produced the following results. It is shown that the dual-consistent refinement preserves a stable convergence rate till the precision is

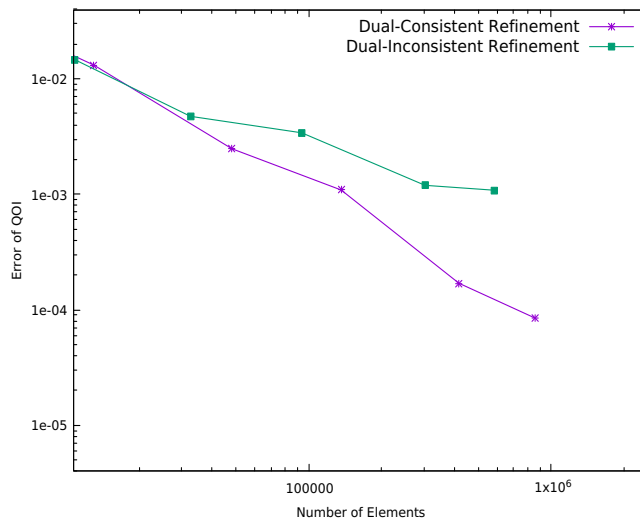


Figure 4: Convergence curves of dual-consistent refinement and dual-inconsistent refinement for NACA0012 with mach number 0.8, attack angle 0° .

below $1.0e-4$ while dual-inconsistent refinement converges to a result around $1.0e-3$ precision. Specifically, in this model,

the error in a dual-consistent framework could converge to 0.00108906 with 136141 elements, while the dual-inconsistent framework converges to 0.00108446 with 581701 elements.

As the configuration for this problem is complicated, the tolerance for the calculation is an important variable. The dual-inconsistent method may refine areas that do not significantly influence the calculation of target functions, resulting in wasted degrees of freedom. As shown in Figure.4, the dual-consistent refinement with 100,000 elements produced approximately equivalent to the dual-inconsistent refinement with nearly 600,000 elements. Compared with the dual-inconsistent refinement, the dual-consistent scheme is always stable, enabling the quantity of interest to converge smoothly. The validity of this assertion has been bolstered through a series of empirical investigations conducted on various models, and the ensuing results are hereby presented.

- A domain with a NACA0012 airfoil, surrounding by an outer circle with a radius of 30;
- Mach number 0.98, and attack angle 1.25°;
- Lax-Friedrichs Numerical Flux;
- Drag coefficient as the quantity of interest, and mirror reflection as the solid wall boundary condition;

In this example, we considered the influence of the attack angle. Since the boundary modification method can help us preserve the adjoint consistency for the reflection boundary condition, the difference between dual consistency and dual inconsistency is shown below.

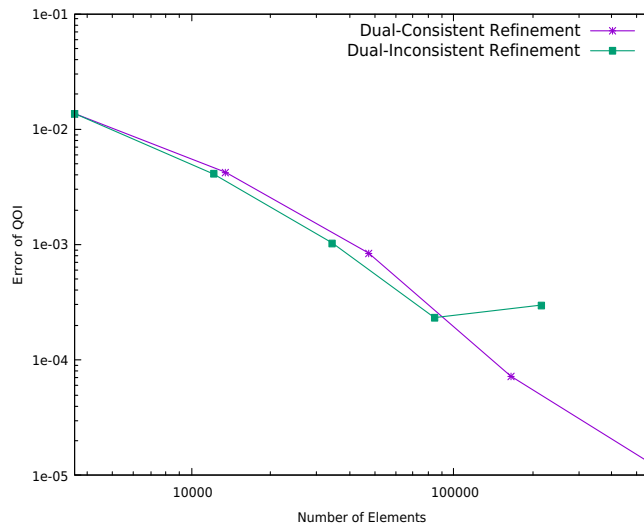


Figure 5: Convergence curves of dual-consistent refinement and dual-inconsistent refinement for NACA0012 with mach number 0.98, attack angle 1.25°.

Even if the error calculated on final meshes derived from dual-consistent refinement and dual-inconsistent refinement have approximate precision, the dual-consistent refinement was more stable than dual-inconsistent refinement. This observation suggests that the accuracy of the quantity of interest improves as the element size increases under a dual-consistent framework. However, the convergence trace of a dual-inconsistent framework has oscillations, not only wasting degrees of freedom but also influencing the analysis of the convergence of target functions. In order to gain a deeper understanding of the efficacy of the DWR method in yielding a stable rate of convergence with respect to the quantity of interest, we have presented a visual analysis of the dual solutions and residuals employed for the computation of the error indicators.

As shown in Figure.6, the residuals of this model oscillated around the shock waves and the direction of the inflow area, while the dual solutions focused on the boundary of the airfoils. The error indicators from the DWR method balance both the residuals and the dual solutions, generating a mesh that could resolve the quantity of interest well. To test the robustness of the dual-consistent framework, we considered different models using the same algorithm in the following parts.

- A domain with a RAE2822 airfoil, surrounding by an outer circle with a radius of 30;
- Mach number 0.729, and attack angle 2.31°;
- Lax-Friedrichs Numerical Flux;
- Drag coefficient as the quantity of interest, and mirror reflection as the solid wall boundary condition;

Similarly, we use a globally refined mesh with 3801088 elements to calculate the quantity of interest, which is $C_d = 0.0144349$. And the dual-consistent framework still works well for the whole algorithm.

Unlike the residual-based adaptation, which emphasizes refinement around shock waves, the DWR method aims to solve the quantity of interest with the least computational cost. In this example, Figure 7 shows that the dual equations

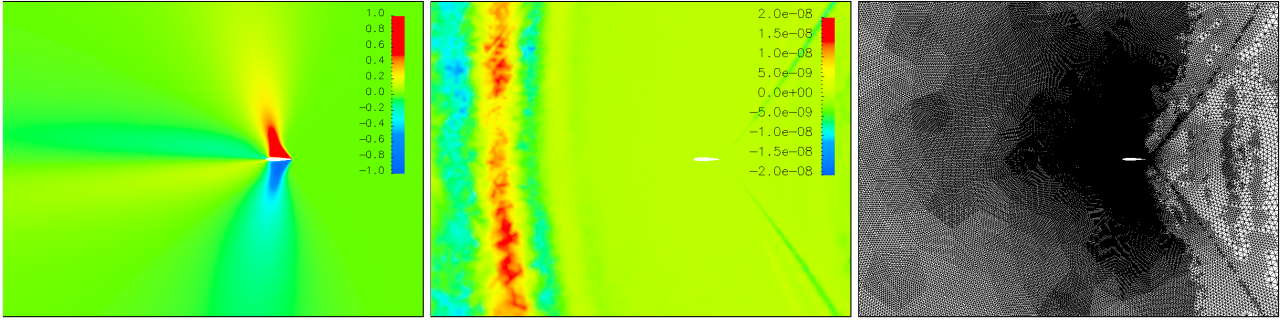


Figure 6: NACA0012 model, Mach number 0.98, attack angle 1.25° : Left: Dual solution of the first variable for the indicators; Middle: Residual of the first variable for the indicators; Right: Meshes generated from the indicators.

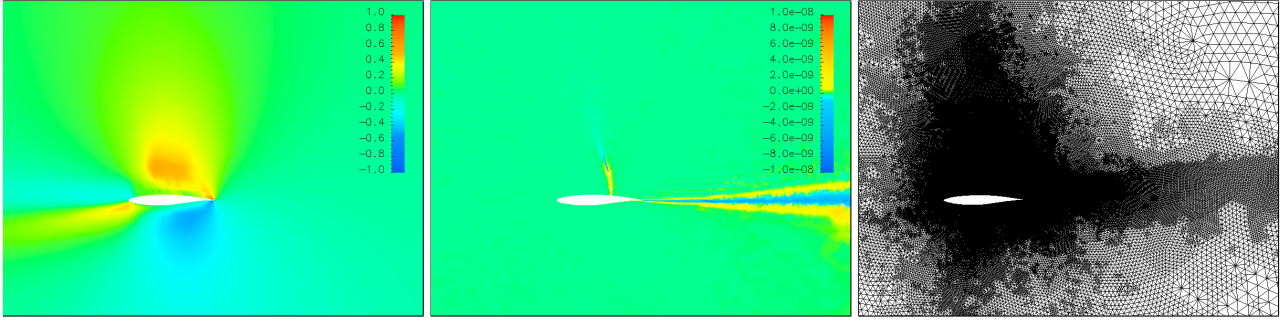


Figure 7: RAE2822 model: Left: Dual solution of the first variable for the indicators; Middle: Residual of the first variable for the indicators; Right: Meshes generated from the indicators.

concentrate on the top half area of the airfoil, while the residuals oscillate around the shock waves and outflow direction. The DWR method combines these two aspects to produce a stable error reduction trace of the target function. The result is shown in Figure.8.

- A domain with two NACA0012 airfoils, surrounding by an outer circle with a radius of 30;
- Mach number 0.8, and attack angle 0° ;
- Lax-Friedrichs Numerical Flux;
- Drag coefficient of different airfoils, and mirror reflection as the solid wall boundary condition;

Initially, we chose the quantity of interest as the drag coefficient of the upper airfoil. Figure 10 exhibits that the dual solutions concentrate on the boundary of the upper airfoil, while the residuals of different variables have oscillations around the shock waves and the outflow direction. The meshes generated from the error indicators predominantly refine the upper airfoil. In contrast, the elements refined around the lower airfoil behave like a residual-based adaptation since the dual equations make no contributions in that region. The upper airfoil took a balance between the dual solutions and the residuals, resulting in a stable convergence of the quantity of interest. Similarly, the quantity of interest is calculated on a mesh with 2227712 elements, then $C_d = 9.218816e - 03$.

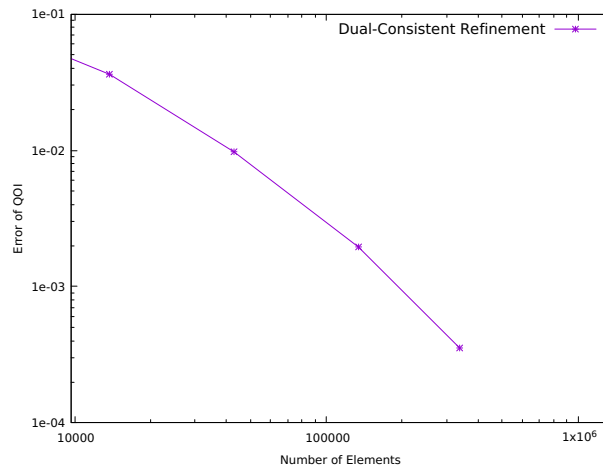


Figure 8: Convergence curves of dual-consistent refinement for RAE2822 with mach number 0.729, attack angle 2.31° .

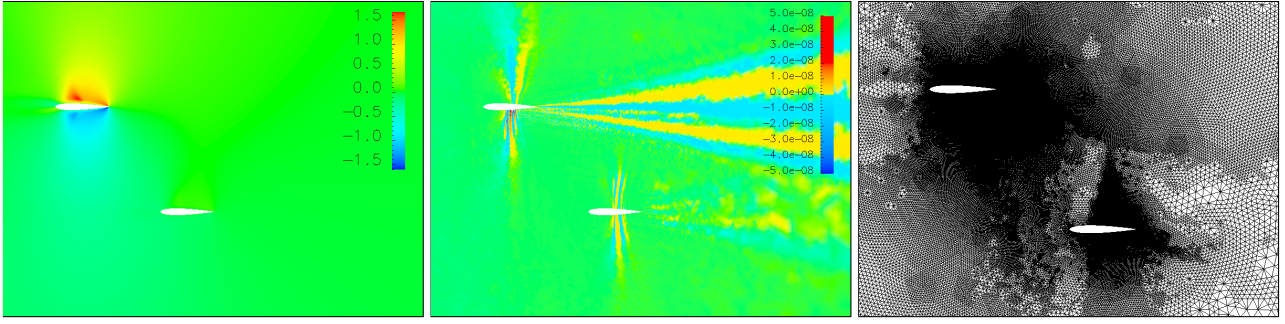


Figure 9: Two bodies model: Left: Dual solution of the first variable for the indicators; Middle: Residual of the first variable for the indicators; Right: Meshes generated from the indicators.

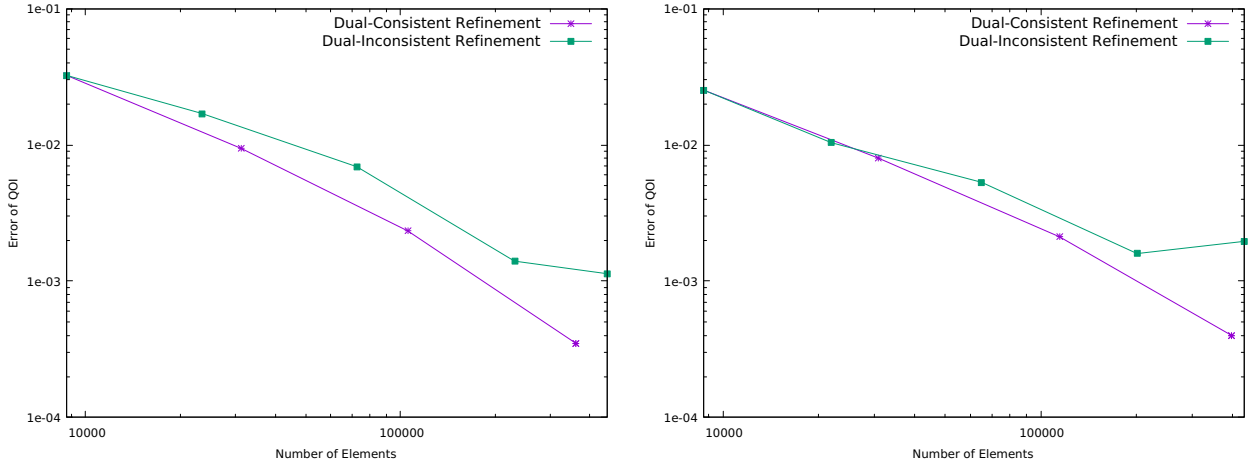


Figure 10: Convergence curves of dual-consistent and dual-inconsistent refinement for Two bodies NACA0012 with mach number 0.8, attack angle 0° . Left: The drag of the upper airfoil chosen as the quantity of interest. Right: The drag of the lower airfoil chosen as the quantity of interest.

If the quantity of interest is chosen as the lower airfoil, the refinement behavior is reversed, with the meshes generated from the error indicators mainly focusing on the lower airfoil.

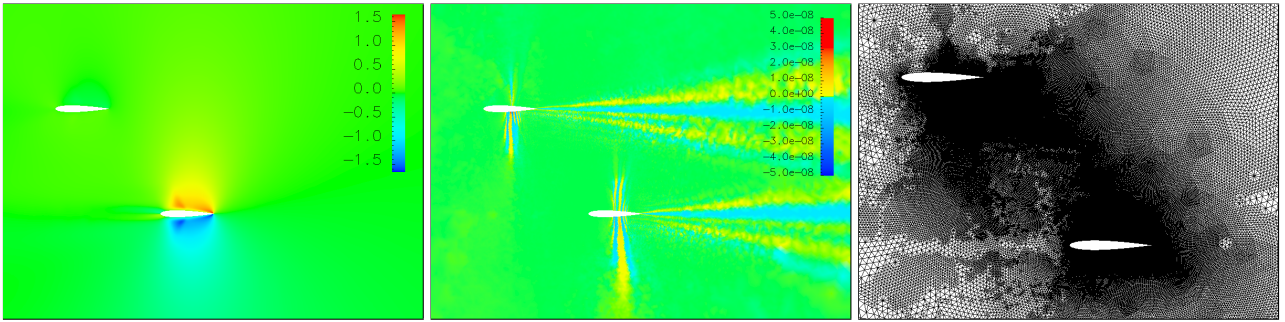


Figure 11: Two bodies model: Left: Dual solution of the first variable for the indicators; Middle: Residual of the first variable for the indicators; Right: Meshes generated from the indicators.

The convergence curves for the two examples demonstrate that dual-consistent refinement is more stable than dual-inconsistent refinement, which can result in unexpected oscillations. More importantly, even if dual-inconsistent DWR may produce a quantity of interest with an acceptable level of precision, it is not always robust enough to derive a satisfactory stopping criterion for target functional-based adaptation.

7 Conclusion

Based on the previous work, we further constructed the h -adaptivity method for the steady Euler equations in the AFVM4CFD package. Implementing the Newton method for nonlinear equations posed a challenge for h -adaptivity, but we validated the dual consistency property using the Newton-GMG solver. Our results showed that under the Newton-GMG framework, a dual-consistent scheme was more stable in obtaining a quantity of interest with expected precision compared with the dual-inconsistent scheme, which could lead to unexpected singularities that would contaminate the refinement area. The dual-consistent framework also offered better precision as the degree of freedom increased. Besides,

to preserve a dual-consistent algorithm, we apply the boundary modification operator for the numerical solutions, allowing for a more generalized configuration for simulations.

However, we encountered some difficulties during the simulations, such as designing a suitable tolerance for mesh adaptations. To make the whole process for refinement more automatic, we plan to develop an algorithm to balance the tolerance based on the mesh in the future. Besides, obtaining the dual solutions still requires a globally refined mesh from the previous step, which we hope to improve upon. As the dual equations are linear equations that do not require high precision to derive the error indicators, machine learning or multiple precisions method will be included to enhance the efficiency in the future. We will also develop a more efficient and faster dual solutions solver based on this framework. Moreover, since the motivation of the DWR based h -adaptivity is from practical issues, the shape optimization techniques shall be discussed in the future. Finally, the dual consistency property for supersonic modeling is still under development.

CRedit authorship contribution statement

Jingfeng Wang: Formal analysis, Methodology, Software, Writing - original draft. **Guanghai Hu:** Conceptualization, Methodology, Software, Supervision, Writing - review & editing.

Declaration of competing interest

The authors declare that they have no known competing financial interests or personal relationships that could have appeared to influence the work reported in this paper.

Acknowledgement

Thanks to the support from National Natural Science Foundation of China (Grant Nos. 11922120 and 11871489), FDCT of Macao S.A.R. (Grant No. 0082/2020/A2), MYRG of University of Macau (MYRG2020-00265-FST) and Guangdong-Hong Kong-Macao Joint Laboratory for Data-Driven Fluid Mechanics and Engineering Applications (2020B1212030001).

References

- [1] M Aftosmis and Marsha Berger. Multilevel error estimation and adaptive h-refinement for cartesian meshes with embedded boundaries. In *40th AIAA Aerospace Sciences Meeting & Exhibit*, page 863, 2002.
- [2] Timothy J Barth and Mats G Larson. A posteriori error estimates for higher order Godunov finite volume methods on unstructured meshes. *Finite Volumes for Complex Applications III, London*, 2002.
- [3] Susanne C Brenner, L Ridgway Scott, and L Ridgway Scott. *The mathematical theory of finite element methods*, volume 3. Springer, 2008.
- [4] Vít Dolejší and Filip Roskovec. Goal-oriented error estimates including algebraic errors in discontinuous Galerkin discretizations of linear boundary value problems. *Applications of Mathematics*, 62(6):579–605, 2017.
- [5] Vít Dolejší and Filip Roskovec. Goal-oriented anisotropic hp-adaptive Discontinuous Galerkin Method for the Euler Equations. *Communications on Applied Mathematics and Computation*, 4:143–179, 2022.
- [6] Krzysztof J Fidkowski and David L Darmofal. Review of output-based error estimation and mesh adaptation in computational fluid dynamics. *AIAA journal*, 49(4):673–694, 2011.
- [7] MBMB Giles, N Pierce, M Giles, and N Pierce. Adjoint equations in CFD-Duality, boundary conditions and solution behaviour. In *13th Computational Fluid Dynamics Conference*, page 1850, 1997.
- [8] Michael B Giles. Discrete adjoint approximations with shocks. In *Hyperbolic problems: theory, numerics, applications*, pages 185–194. Springer, 2003.
- [9] Michael B Giles, Mihai C Duta, Jens-Dominik Muller, and Niles A Pierce. Algorithm developments for discrete adjoint methods. *AIAA journal*, 41(2):198–205, 2003.
- [10] Wenrui Hao, Jonathan D Hauenstein, Chi-Wang Shu, Andrew J Sommese, Zhiliang Xu, and Yong-Tao Zhang. A homotopy method based on WENO schemes for solving steady state problems of hyperbolic conservation laws. *Journal of Computational Physics*, 250:332–346, 2013.
- [11] Kathryn Harriman, DJ Gavaghan, and Endre Suli. The importance of adjoint consistency in the approximation of linear functionals using the discontinuous Galerkin finite element method. 2004.
- [12] Ralf Hartmann. Adjoint consistency analysis of discontinuous Galerkin discretizations. *SIAM Journal on Numerical Analysis*, 45(6):2671–2696, 2007.

- [13] Ralf Hartmann and Tobias Leicht. Generalized adjoint consistent treatment of wall boundary conditions for compressible flows. *Journal of Computational Physics*, 300:754–778, 2015.
- [14] Jason E Hicken and David W Zingg. Dual consistency and functional accuracy: a finite-difference perspective. *Journal of Computational Physics*, 256:161–182, 2014.
- [15] Guanghui Hu. An adaptive finite volume method for 2D steady Euler equations with WENO reconstruction. *Journal of Computational Physics*, 252:591–605, 2013.
- [16] Guanghui Hu, Ruo Li, and Tao Tang. A robust WENO type finite volume solver for steady Euler equations on unstructured grids. *Communications in Computational Physics*, 9(3):627–648, 2011.
- [17] Guanghui Hu, Xucheng Meng, and Nianyu Yi. Adjoint-based an adaptive finite volume method for steady Euler equations with non-oscillatory k-exact reconstruction. *Computers & Fluids*, 139:174–183, 2016.
- [18] Guanghui Hu and Nianyu Yi. An adaptive finite volume solver for steady Euler equations with non-oscillatory k-exact reconstruction. *Journal of Computational Physics*, 312:235–251, 2016.
- [19] Antony Jameson. Solution of the Euler equations for two dimensional transonic flow by a multigrid method. *Applied Mathematics and Computation*, 13(3):327–355, 1983.
- [20] Antony Jameson. Aerodynamic design via control theory. *Journal of Scientific Computing*, 3:233–260, 1988.
- [21] Antony Jameson and Timothy J. Baker. Solution of the Euler equations for complex configurations. 1983.
- [22] Antony Jameson, W. Schmidt, and Eli Turkel. Solutions of the Euler Equations by Finite Volume Methods Using Runge-Kutta Time-Stepping Schemes. *AIAA paper*, 1259, 1981.
- [23] Gaetan K.W. Kenway, Charles A. Mader, Ping He, and Joaquim R.R.A. Martins. Effective adjoint approaches for computational fluid dynamics. *Progress in Aerospace Sciences*, 110:100542, 2019.
- [24] Boya Li. Newton linearized methods for semilinear parabolic equations. *Numerical Mathematics-theory Methods and Applications*, 13:928–945, 2020.
- [25] Ruo Li, Xin Wang, and Weibo Zhao. A multigrid block LU-SGS algorithm for Euler equations on unstructured grids. *Numerical Mathematics: Theory, Methods and Applications*, 1:92–112, 2008.
- [26] Ruo Li and Wei Zhong. A modified adaptive improved mapped weno method. *Communications in Computational Physics*, 30(5):1545–1588, 2021.
- [27] Liu, YangyangYang, LimingShu, Chang, Zhang, and Huangwei. A multi-dimensional shock-capturing limiter for high-order least square-based finite difference-finite volume method on unstructured grids. *Advances in Applied Mathematics and Mechanics*, 13(3):671–700, 2020.
- [28] James Lu. *An a posteriori error control framework for adaptive precision optimization using discontinuous Galerkin finite element method*. PhD thesis, Massachusetts Institute of Technology, 2005.
- [29] Xucheng Meng, Yaguang Gu, and Guanghui Hu. A Fourth-Order Unstructured NURBS-Enhanced finite volume WENO Scheme for Steady Euler Equations in Curved Geometries. *Communications on Applied Mathematics and Computation*, pages 1–28, 2021.
- [30] Xucheng Meng and Guanghui Hu. A nurbs-enhanced finite volume method for steady euler equations with goal-oriented h -adaptivity. *Communications in Computational Physics*, 32:490–523, 06 2022.
- [31] Marian Nemeč, Michael Aftosmis, and Mathias Wintzer. Adjoint-based adaptive mesh refinement for complex geometries. In *46th AIAA Aerospace Sciences Meeting and Exhibit*, page 725, 2008.
- [32] Niles A Pierce and Michael B Giles. Adjoint recovery of superconvergent functionals from PDE approximations. *SIAM review*, 42(2):247–264, 2000.
- [33] Ajay Rangarajan, Georg May, and Vit Dolejši. Adjoint-based anisotropic hp-adaptation for discontinuous galerkin methods using a continuous mesh model. *Journal of Computational Physics*, 409:109321, 2020.
- [34] Jeffrey P Slotnick, Abdollah Khodadoust, Juan Alonso, David Darmofal, William Gropp, Elizabeth Lurie, and Dimitri J Mavriplis. CFD vision 2030 study: a path to revolutionary computational aerospace. Technical report, 2014.
- [35] David A Venditti and David L Darmofal. Adjoint error estimation and grid adaptation for functional outputs: Application to quasi-one-dimensional flow. *Journal of Computational Physics*, 164(1):204–227, 2000.
- [36] David A Venditti and David L Darmofal. Grid adaptation for functional outputs: application to two-dimensional inviscid flows. *Journal of Computational Physics*, 176(1):40–69, 2002.
- [37] Shuhai Zhang, Shufen Jiang, and Chi-Wang Shu. Improvement of convergence to steady state solutions of Euler equations with the WENO schemes. *Journal of Scientific Computing*, 47(2):216–238, 2011.